was monitored with a Luciferase Assay Kit (Promega) and luminometer (Lumat LB 9507, Berthold). The results were expressed as light units per milligram of cell protein determined by a micro BCA assay kit (Pierce).

Results and discussion

Heterobifunctional PEGs bearing 4-vinylbenzyl group at the α-end and a carboxylic acid at the ω-end (CH_2=CH–Ph–PEG–COOH, M_n=1,800 and 8,000) were synthesized, in accordance with our literature [21]. The introduction of a lactose group to the carboxylic acid end of CH_2=CH–Ph–PEG–COOH (M_n=8,000) was performed by the reaction with *p*-aminophenyl-β-D-lactopyranoside in the presence of an excess amount of NHS and EDC in 25 mM MES buffer, pH 6.5, at room temperature for 24 h. Based on the hydrogen nuclear magnetic resonance (^{1}H NMR) spectrum of CH_2=CH–Ph–PEG–lactose (Fig. 2), the lactose molecules were almost quantitatively introduced to the PEG chain end as determined by the integral ratio between the ester metylene protons (4.1 ppm, 2H, PEG–CH_2CH_2–O–CO–CH_2–) and the phenyl protons of the lactose moiety (6.9 ppm, 2H, –CO–NH–Ph–lactose). Lactosylated and nonlactosylated nanogels were prepared at room temperature by means of the emulsion polymerization of 2-(*N,N*-diethylamino)ethyl methacrylate (AMA) with CH_2=CH–Ph–PEG–lactose (M_n=8,000) or CH_2=CH–Ph–PEG–COOH (M_n=1,800 or 8,000) in the presence of KPS and EGDMA (0.1 or 1 mol%) as a cross-linker because the tertiary amino groups in the AMA monomer and KPS spontaneously forms a redox complex (initiator) at room temperature through the electron transfer from AMA to KPS. The characterizations of the obtained nanogels with a unimodal size distribution (μ_2/Γ^2<0.15) are summarized in Table 1.

An MTT assay was done using HuH-7 cells (human hepatoma cells) possessing ASGP receptors, which recognize compounds bearing terminal galactose moieties [22, 23], to evaluate the cytotoxicity of the obtained nanogels, as shown in Fig. 3. Nanogel-2k-1.0% with short PEG chains (M_n=1,800) and nanogel-8k-0.1% with low cross-linking density showed high cytotoxicity in a dose-dependent manner, despite possessing PEG chains surrounding the cross-linked PAMA core: The 50% cytotoxicity concentrations were determined to be ca. 10 and 6 μg/ml, respectively. In addition, the viability of cells treated with HCQ was less than 50% at 100 μM (=31.4 μg/ml). In sharp contrast, nanogel-8k-1.0% and lac-nanogel-8k-1.0% with long PEG chains (M_n=8,000) and moderate cross-linking density (1.0%) showed low cytotoxicity even at 100 μg/ml (>70% cell viability). These results suggest that the cytotoxicity of the nanogels obviously depended on the chain length of the PEG and the cross-linking density of the PAMA core. The observed high cytotoxicity of nanogel-2k-1.0% and nanogel-8k-0.1% is most likely due to partial exposure of the PAMA core to the outside and/or the existence of dangling PAMA chains, as the zeta potential of the fully protonated nanogel-2k-1.0% and nanogel-8k-0.1% at pH 5 was found to be +32.3 and +33.1 mV, respectively. On the contrary, nanogel-8k-1.0% and lac-nanogel-8k-1.0% with longer PEG

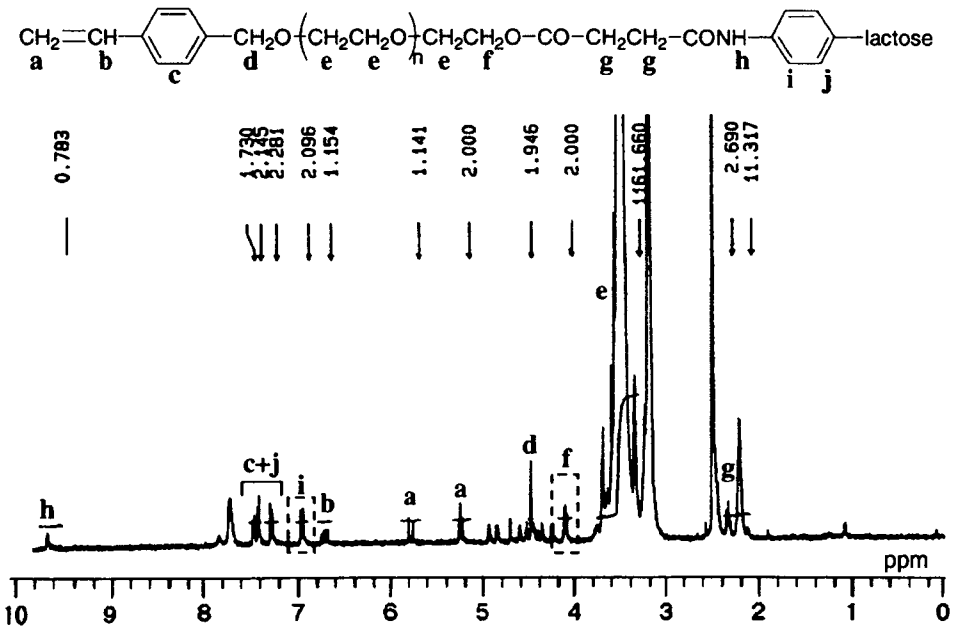

Fig. 2 ^{1}H NMR spectrum of the CH_2=CH–Ph–PEG–lactose in DMSO-d_6 at 55 °C (peaks at 2.5 and 3.2 ppm are attributed to the DMSO and water, respectively)

Table 1 The nanogel samples used in this study

Samples	M_n(PEG)[a]	Cross-linker[b] (mol %)	Particle size[c] (nm)	
			pH 6	pH 8
Nanogel-2k-1.0%	1,800	1.0	128.9	72.0
Nanogel-8k-0.1%	8,000	0.1	320.0	89.3
Nanogel-8k-1.0%	8,000	1.0	152.7	84.4
Lac-nanogel-8k-1.0%	8,000	1.0	160.8	84.7

[a] Determined by SEC chromatography
[b] Feed molar ratio of cross-linking agents: EGDMA
[c] Determined by DLS analysis

chains (M_n=8,000) and higher cross-linking density (1.0%) showed the effective compartmentalization of the cross-linked PAMA core surrounded by long PEG chains to prevent both exposure of the PAMA core to the outside and the formation of dangling PAMA chains (fully protonated nanogel-8k-1.0%, ζ=+14.0 mV), leading to the low cytotoxicity of these nanogels.

To estimate the endosomolytic ability of the nanogels, a transfection study of the PEG-*b*-PLL/pDNA polyplex micelle was carried out in the presence and absence of lac-nanogel-8k-1.0% (100 μg/ml) using HuH-7 cells, although there is no interaction between the polyplex micelle and nanogel due to the existence of the tethered PEG chains (PEG shell). PEG-*b*-PLL/pDNA polyplex micelles were prepared at N/P=2, where the highest transfection efficiency and complete DNA condensation were observed in our previous study [5]. As can be seen in Fig. 4, the PEG-*b*-PLL/pDNA polyplex micelle alone

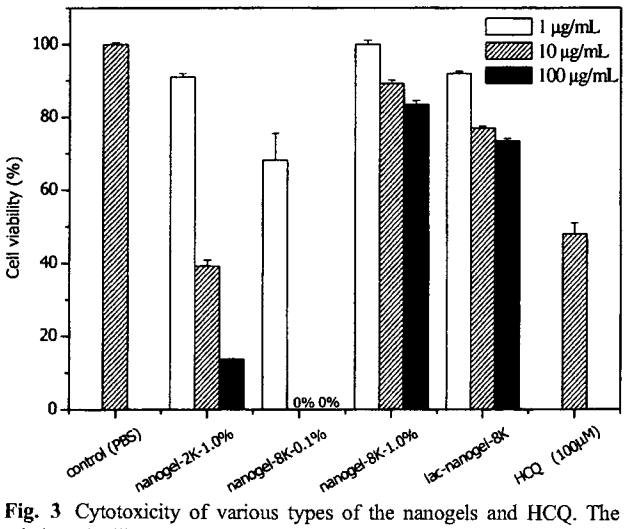

Fig. 3 Cytotoxicity of various types of the nanogels and HCQ. The relative viability of HuH-7 cells is expressed as functions of nanogel concentrations: 1 μg/ml (*open bars*), 10 μg/ml (*gray bars*), and 100 μg/ml (*filled bars*). The results are expressed as means±SEM, n=8

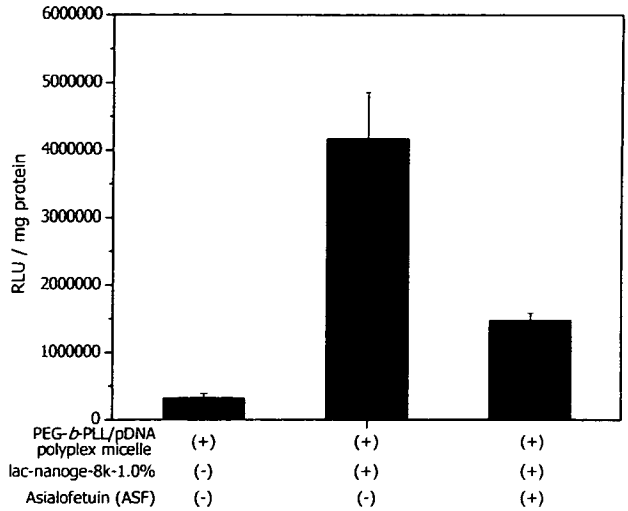

Fig. 4 Efficiency of transfection into HuH-7 cells of the PEG-*b*-PLL/pDNA polyplex micelles prepared at N/P=2. The lac-nanogel-8k-1.0% (100 μg/ml) and ASF (1.5 mg/ml) were used. The results are expressed as means±SEM, n=4

(without lac-nanogel-8k-1.0%) showed only limited transfection efficiency without any cytotoxicity due to the lack of the endosomal escape function, leading to the lysosomal degradation of the pDNA. In sharp contrast, the PEG-*b*-PLL/pDNA polyplex micelle with lac-nanogel-8k-1.0% achieved a significant increase in transfection efficiency compared with the PEG-*b*-PLL/pDNA polyplex micelle alone, viz., the transfection efficiency was found to be 3.2×10^5 (RLU/mg protein) and 4.2×10^6 (RLU/mg protein) for the PEG-*b*-PLL/pDNA polyplex micelle alone and the PEG-*b*-PLL/pDNA polyplex micelle with the lac-nanogel-8k-1.0%, respectively. This almost 13-fold increase in transfection efficiency in lac-nanogel-8k-1.0% is remarkable because other polyplex micelle system in the presence of HCQ (100 μM) showed the 10- and 15-fold enhancement of the transfection efficiency for the HuH-7 cells (same cell line) [19] and HepG2 cells [4], respectively. In addition, significant increase in the transfection efficiency of the PEG-*b*-PLL/pDNA polyplex micelle with nanogel-8k-1.0% was also observed for 293T cells (human kidney; see Fig. S2). These results suggest that after the partial co-internalization of the PEG-*b*-PLL/pDNA polyplex micelle and lac-nanogel-8k-1.0% into the HuH-7 cells, the protonation of the PAMA core of lac-nanogel-8k-1.0% occurred in synchronously with the pH decrease in the endosomal compartment (pH=6~5), leading to the significant swelling of the PAMA core of lac-nanogel-8k-1.0% (pH=8.0, 84.7 nm → pH=6.0, 160.8 nm in Table 1) to increase the ion osmotic pressure (buffer effect). This may induce the disruption of the endosome, facilitating the transport of the co-internalized PEG-*b*-PLL/pDNA polyplex micelle into the cytoplasm.

To examine whether the lactose moiety (galactose terminal) on the surface of lac-nanogel-8k-1.0% is recognized by the ASGP receptors existing on the HuH-7 cells, a transfection study of the PEG-*b*-PLL/pDNA polyplex micelle with lac-nanogel-8k-1.0% was also performed in the presence of ASF. Note that the ASF is known to strongly interact with ASGP receptors, viz., ASF acts as a competitive inhibitor of the ASGP receptor-mediated endocytosis [24]. A significant decrease in the transfection efficiency of the PEG-*b*-PLL/pDNA polyplex micelle with lac-nanogel-8k-1.0% was observed in the presence of ASF, indicating that the cellular association and internalization of lac-nanogel-8k-1.0% along with the PEG-*b*-PLL/pDNA polyplex micelle occur mainly through the ASGP receptor-mediated process, which is inhibited in the presence of ASF. Thus, it seems reasonable to conclude that an appreciable fraction of the lac-nanogel-8k-1.0% along with the PEG-*b*-PLL/pDNA polyplex micelle is taken up by HuH-7 cells through the ASGP receptor-mediated endocytosis process mediated by the cluster of a large number of lactose moieties on the surface of the lac-nanogel-8k-1.0%, followed by the effective disruption of the endosome by the buffer effect of the unprotonated PAMA core in lac-nanogel-8k-1.0%.

In conclusion, the pH-responsive and targetable PEGylated nanogel (lac-nanogel-8k-1.0%) constructed from a cross-linked polyamine core and tethered PEG chains bearing a lactose molecule exhibited significant endosomolytic ability, achieving the pronounced transfection efficiency of the PEG-*b*-PLL/pDNA polyplex micelles without any cytotoxicity. Therefore, the pH-responsive and targetable PEGylated nanogel thus described in this paper would be a promising targetable and biocompatible endosomolytic agent for nonviral gene delivery systems.

References

1. Yang Y, Li Q, Ertl HC, Wilson JM (1995) J Virol 69:2004–2015
2. Yang Y, Li Q, Ertl HC, Wilson JM (1994) Immunity 1:433–442
3. Gunter KC, Khan AS, Noguchi PD (1993) Hum Gene Ther 4:643–645
4. Wakebayashi D, Nishiyama N, Itaka K, Miyata K, Yamasaki Y, Harada A, Koyama H, Nagasaki Y, Kataoka K (2004) Biomacromolecules 5:2128–2136
5. Itaka K, Yamauchi K, Harada A, Nakamura K, Kawaguchi H, Kataoka K (2003) Biomaterials 24:4495–4506
6. Itaka K, Yamauchi K, Harada A, Nakamura K, Kawaguchi H, Kataoka K (2002) Biomacromolecules 3:841–845
7. Harada-Shiba M, Yamauchi K, Harada A, Takamisawa I, Shimokado K, Kataoka K (2002) Gene Ther 9:407–417
8. Kataoka K, Harada A, Wakebayashi D, Nagasaki Y (1999) Macromolecules 32:6892–6894
9. Katayose S, Kataoka K (1998) J Pharm Sci 87:160–163
10. Katayose S, Kataoka K (1997) Bioconjug Chem 8:702–707
11. Wakebayashi D, Nishiyama N, Yamasaki Y, Itaka K, Kanayama N, Harada A, Nagasaki Y, Kataoka K (2004) J Control Release 95:653–664
12. Brown MD, Schatslein AG, Uchegbu IF (2001) Int J Pharm 229:1–21
13. Nishikawa M, Huang L (2001) Hum Gene Ther 12:861–870
14. Gruenberg J (2001) Nat Rev Mol Cell Biol 2:721–730
15. Clague MJ (1998) Biochem J 336:271–282
16. Mukherjee S, Ghosh RN, Maxfield FR (1997) Endocytosis. Physiol Rev 77:759–803
17. Duncan R (1992) Anti-Cancer Drugs 3:175–210
18. Boussif O, Lezoualc F, Zanta MA, Mergny MD, Scherman D, Demeneix B, Behr JP (1995) Proc Natl Acad Sci USA 92:7297–7301
19. Oishi M, Kataoka K, Nagasaki Y (2006) Bioconjug Chem 17:677–688
20. Fukushima S, Miyata K, Nishiyama N, Kanayama N, Yamasaki Y, Kataoka K (2005) J Am Chem Soc 127:2810–2811
21. Hayashi H, Iijima M, Kataoka K, Nagasaki Y (2004) Macromolecules 37:5389–5396
22. Hashida M, Takemura S, Nishikawa M, Takakura Y (1998) J Control Release 53:301–310
23. Stockert RJ (1995) Physiol Rev 75:591–609
24. Zanta MA, Boussif O, Adib A, Behr JP (1997) Bioconjug Chem 8:839–844

Density Control of Poly(ethylene glycol) Layer To Regulate Cellular Attachment

Tomomi Satomi,[†,‡,§,∥] Yukio Nagasaki,[⊥] Hisatoshi Kobayashi,[§] Hidenori Otsuka,[*,†,‡,§] and Kazunori Kataoka[∥,#]

Department of Applied Chemistry, Faculty of Science, Tokyo University of Science, 1-3 Kagurazaka, Shinjuku-ku, Tokyo 162-8601, Japan, Division of Bioengineering and Bioinformatics, Graduate School of Information Science and Technology, Hokkaido University, North 14 West 9, Sapporo 060-0814, Japan, Biomaterials Center, National Institute for Materials Science (NIMS), 1-1 Namiki, Tsukuba, Ibaraki 305-0044, Japan, Division of Clinical Biotechnology, Center for Disease Biology and Integrative Medicine, Graduate School of Medicine, The University of Tokyo, 7-3-1 Hongo, Bunkyo-ku, Tokyo 113-0033, Japan, Graduate School of Pure and Applied Sciences, University of Tsukuba, 1-1-1 Tenodai, Tsukuba, Ibaraki 305-8571, Japan, and Department of Materials Science and Engineering, Graduate School of Engineering, The University of Tokyo, 7-3-1 Hongo, Tokyo 113-8656, Japan

Received August 17, 2006. In Final Form: March 7, 2007

A wide variety of cells usually integrate and respond to the microscale environment, such as soluble protein factors, extracellular matrix proteins, and contacts with neighboring cells. To gain insight into cellular microenvironment design, we investigated two-dimensional microarray formation of endothelial cells on a micropatterned poly(ethylene glycol) (PEG)-brushed surface, based on the relationship between PEG chain density and cellular attachment. The patterned substrates consisted of two regions: the PEG surface that acts as a cell-resistant layer and the exposed substrate surface that promotes protein or cell adsorption. A PEG-brushed layer was constructed on a gold substrate using PEG with a mercapto group at the end of the chain. The density of the PEG-brushed layer increased substantially with repetitive adsorption/rinse cycles of PEG on the gold substrate, allowing marked reduction of nonspecific protein adsorption. These repeated adsorption/rinse cycles were further regulated by using longer (5 kDa) and shorter (2 kDa) PEG to construct PEG layers with different chain density, and subsequent micropatterning was achieved by plasma etching through a micropatterned metal mask. The effects of PEG chain density on pattern formation of cell attachment were determined on micropatterning of endothelial cells. The results indicated that cell pattern formation was strongly dependent on the PEG chain density and on the extent of protein adsorption. Notably, a PEG chain density high enough to inhibit outgrowth of endothelial cells from the cell-adhering region in the horizontal direction could be obtained only by employing formation of a short filler layer of PEG in the preconstructed longer PEG-brushed layer, which prevented nonspecific protein adsorption almost completely. In this way, a completely micropatterned array of endothelial cells with long-term viability was obtained. This clearly indicated the importance of a short underbrushed PEG layer in minimizing nonspecific protein adsorption for long-term maintenance of the active cell pattern. The strategy for cell patterning presented here can be employed in tissue engineering to study cell−cell and cell−surface interactions. It is also applicable for high-throughput screening and clinical diagnostics, as well as interfacing cellular and microfabricated components of biomedical microsystems.

Introduction

Surface engineering techniques for cellular micropatterning are emerging as important tools to clarify the effects of the microenvironment on cellular behavior,[1,2] as cells usually integrate and respond to the microscale environment, such as chemical and mechanical properties of the surrounding fluid and extracellular matrix, soluble protein factors, small signal molecules, and contacts with neighboring cells.[3,4] Furthermore, living cells undergo physiological changes in response to exposure to drugs and environmental perturbations, such as toxins, pathogens, or other agents, and thus high-throughput technologies using whole cells have also been developed.[5−13] To develop this kind of cellular microarray composed of a cell-resistant surface and cell attachment region, micropatterning a protein-repellent surface is important because cellular adhesion and proliferation are regulated by protein adsorption.

* Corresponding author. Address: Hidenori Otsuka, Ph.D., Department of Applied Chemistry, Faculty of Science, Tokyo University of Science, 1-3 Kagurazaka, Shinjuku-ku, Tokyo 162-8601, Japan. Phone: +81-3-5228-8265. Fax: +81-3-5228-8265. E-mail: h.otsuka@rs.kagu.tus.ac.jp.

† Tokyo University of Science.

‡ Hokkaido University.

§ National Institute for Materials Science.

∥ Graduate School of Medicine, The University of Tokyo.

⊥ University of Tsukuba.

Graduate School of Engineering, The University of Tokyo.

(1) Whitesides, G. M.; Ostuni, E.; Takayama, S.; Jiang, X.; Ingber, D. E. *Annu. Rev. Biomed. Eng.* **2001**, *3*, 335.

(2) Jeon, N. L.; Baskaran, H.; Detringer, S. K. W.; Whitesides, G. M.; Van de Water, L.; Toner, M. *Nat. Biotechnol.* **2002**, *20*, 826.

(3) Zamir, E.; Katz, B. Z.; Aota, K. M.; Yamada, K. M.; Geiger, B.; Kam, Z. *J. Cell Sci.* **1999**, *112*, 1655.

(4) Geiger, B.; Bershadsky, R.; Pankov, R.; Yamada, K. M. *Nat. Rev. Mol. Cell Biol.* **2001**, *2*, 793.

(5) Stenger, D. A.; Gross, G. W.; Keefer, E. W.; Shaffer, K. M.; Andreadis, J. D.; Ma, W.; Pancrazio, J. J. *Trends Biotechnol.* **2001**, *19*, 304.

(6) Kononen, J.; Bubendorf, L.; Kallioniemi, A.; Barlund, M.; Schraml, P.; Leighton, S.; Torhorst, J.; Mihatsch, M. J.; Sauter, G.; Kallioniemi, O. P. *Nat. Med.* **1998**, *4*, 844.

(7) Ziauddin, J.; Sabatini, D. M. *Nature* **2001**, *411*, 107.

(8) Michalopoulos, G. K.; DeFrances, M. C. *Science* **1997**, *276*, 60.

(9) Anderson, D. G.; Levenberg, S.; Langer, R. *Nat. Biotechnol.* **2004**, *22*, 863.

(10) Revzin, A.; Tompkins, R. G.; Toner, M. *Langmuir* **2003**, *19*, 9855.

(11) Thielecke, H.; Mack, A.; Robitzki, A. *Biosens. Bioelectron.* **2001**, *16*, 261.

(12) Mack, A. R.; Thielecke, H.; Robitzki, A. A. *Trends Biotechnol.* **2002**, *20*, 56.

(13) Otsuka, H.; Hirano, A.; Nagasaki, Y.; Okano, T.; Horiike, Y.; Kataoka, K. *ChemBioChem* **2004**, *5*, 850.

10.1021/la0624384 CCC: $37.00
Published on Web 05/05/2007

A number of approaches to construct protein-repellent and subsequent cell-repellent surfaces have been studied using polymer coating. In fact, there has been a great deal of discussion regarding the molecular properties on the surface, and it is widely believed that effective protein rejection requires the bound polymer to be heavily hydrated, densely packed, neutral, deposited in a thick layer, and conformationally mobile.[14-18] Here, we focus on poly(ethylene glycol) (PEG), one of the most useful polymers to repel protein. Surface modification by PEG leads to a significant reduction in the nonspecific interaction of biological molecules with the surface due to its high degree of hydrophilicity and chain flexibility, inducing an effective exclusion volume effect.[19-22] Most previous studies of surfaces with immobilized PEG have described higher protein-repellent ability with longer chain, resulting in increasing thickness of PEG,[23-27] which is considered to be due to the stronger attenuation of the long-range Lifshitz–van der Waals attraction. However, immobilization of longer PEG chains results in a decrease in chain density due to its larger exclusion volume effect, although it has a sufficiently large separation between the surface and proteins. Conversely, immobilization of shorter PEG chains gives higher density due to its smaller exclusion volume effect, although it has a smaller separation between the surface and proteins. To resolve this controversial issue of the length and density of the PEG layer, we previously reported the development of surface construction using long and short PEG chains; formation of a short, filler layer of PEG in the preconstructed longer PEG-brushed layer prevented nonspecific protein adsorption almost completely.[28] In most studies of this type, a protein-repellent surface will be expected to repel cellular attachment. However, the question of how dense the immobilized PEG chain must be to control cell attachment has still not been answered.

The present study was performed to determine the influence of PEG chain density on cellular attachment directly. For the micropatterning of cells, it is necessary to prevent overgrowth of cells from the cell-adhering pattern; i.e., construction of a cytophobic surface is important for micropatterning. Here, we controlled the modification ratio of long and short PEG chains to construct surfaces with different PEG chain densities, and subsequent micropatterning was achieved by plasma etching through a micropatterned metal mask (ϕ = 100 μm, edge-to-edge spacing of l = 300 μm). The relationship between PEG chain density and cellular attachment is discussed on micropatterning of endothelial cells.

Experimental Section

Materials. Poly(ethylene glycol) (PEG) with a methoxy group at one end and a mercapto group at the other (MeO–PEG–SH) was provided by NOF Corporation (Tokyo, Japan). The molecular weight and polydispersity of PEGs, denoted by PEG2k and PEG5k, were 2096 and 1.05 and 5341 and 1.04, respectively. Gold chips (SIA KIT Au) for SPR measurements were purchased from Biacore AB (Uppsala, Sweden). Human umbilical endothelial cells (HUVEC) were purchased from Cambrex (Cambrex BioScience Walkersville, Inc., Walkersville, MD). HUVECs were cultured in EBM-2 medium (Cambrex). Water used in this study was purified by passing it through a Milli-Q System (Nihon Millipore Co., Tokyo, Japan) until its specific conductivity fell below 0.1 μS cm^{-1}.

1. PEG Immobilization Study. *Preparation of MeO–PEG–SH-Modified Gold Surface.* Immobilization of PEG on the gold sensor chip surface was performed using a surface plasmon resonance (SPR) instrument (Biacore X; Biacore AB, Uppsala, Sweden). Phosphate buffered saline (PBS; pH 7.4, 0.15 M, containing 1 M NaCl) solutions of PEG were injected at a flow rate of 10 μL/min for 10 min at 37 °C under running PBS (pH 7.4, 0.15 M, containing 1 M NaCl). An SPR sensorgram on the gold sensor chip for this adsorption/rinsing (with running PBS) of PEG was monitored, and the amount of immobilized PEG was assessed by the SPR angle shift. PEG solutions with different concentrations were injected on a sensor chip, and then the plateau region for PEG immobilization was determined. To increase (or change) the amount of immobilized PEG, the process of PEG injection was repeated several times according to the reported method.[24] PEGylated surfaces prepared by one, two, and three repetitive injections were denoted as PEG5k(1), PEG5k(2), and PEG5k(3) surfaces, respectively. In a manner similar to the above-repeated process, successive PEGylation with longer and then shorter PEG was carried out. A shorter PEG (PEG2k) as a filler was layered on the surface with the preconstructed longer PEG brushes (PEG5k) by repetitive injection. PEG5k(1) surfaces with three treatments with the filler PEG and PEG5k(2) with four treatments with the filler PEG were denoted as PEG5k(1)/2k(3) and PEG5k(2)/2k(4) surfaces, respectively.

The density of immobilized PEG chains was estimated quantitatively by quartz crystal microbalance (QCM) measurement using an AT-cut gold-sputtered quartz crystal with a resonance frequency of 27 MHz (Initium Inc., Japan). The frequency was recorded after immersing the crystals in the PBS (pH 7.4, 0.15 M, containing 1 M NaCl) at 37 °C. After baseline stabilization, PEG solutions (PEG5k, PEG2k) were injected at a concentration of 0.01 mg/mL, which was optimized above in the same repetitive manner as in SPR measurement (PEG5k(3), PEG5k(1)/2k(3), PEG5k(2)/2k(4)).

Surface Characterization. The wettability of all PEGylated surfaces was estimated from the static and dynamic contact angle measurements (CA-W contact angle meter; Kyowa Interface Science Co., Ltd., Tokyo, Japan).[29] Gold and PEGylated gold surfaces were constructed on glass substrates as described in detail in the section describing the cell culture study (see "Construction of PEGylated surface"). Water-in-air and air-in-water systems were applied in the static contact angle measurements. Water-in-air system measurement was performed by a sessile droplet technique, where a water droplet (Milli-Q quality) was placed on the sample surface at 25 °C. The air-in-water system procedure followed the captive bubble technique, where the sample surface was immersed in water maintained at 25 °C and a small air bubble was placed on the sample surface from the bottom using a curved needle. The contact angle of each surface was measured on 10 spots, and the obtained values were averaged.

For dynamic contact angle measurements, the advancing (θ_{adv}) and receding (θ_{rec}) contact angles were obtained by extending and then contracting the volume (5.9 μL) of the water droplet using a motor-driven syringe at a rate of 1.88 μL/s for 3.1 s. The extending/contracting droplet was monitored with a CCD camera; each picture was captured every 67 ms, and 24 images were taken for both θ_{adv} and θ_{rec}, when the water droplet volume was changed at 1.88 μL/s. The contact angles were evaluated from video printouts of the droplet.

(14) Lee, J. H.; Kopeckova, P.; Kopecek, J.; Andrade, J. D. *Biomaterials* **1990**, *11*, 455.
(15) Desai, N. P.; Hubbell, J. A. *Macromolecules* **1992**, *25*, 226.
(16) Bergstrom, K.; Osterberg, E.; Holmberg, K.; Riggs, J. A.; Van Alstime, J. M.; Schuman, T. P.; Burns, N. L.; Harris, J. M. *Colloids Surf. A* **1993**, *77*, 159.
(17) Sofia, S. J.; Premnath, V.; Merrill, E. W. *Macromolecules* **1998**, *31*, 5059.
(18) Osterberg, E.; Bergstrom, K.; Holmberg, K.; Schuman, T. P.; Riggs, J. A.;. Burns, N. L; Van Alstine, J. M.; Harris, J. M. *J. Biomed. Mater. Res.* **1995**, *29*, 741.
(19) Mori, Y.; Nagaoka, S.; Takiuchi, H.; Kikuchi, T.; Noguchi, N.; Tanzawa, H.; Noishiki, Y. *Trans. Am. Soc. Artif. Internal Organs* **1982**, *28*, 459.
(20) Bergstrom, K.; Osterberg, E.; Holmberg, K.; Hoffman, A. S.; Schuman, T. P.; Kozlowski, A.; Harris, J. M. *J. Biomater. Sci. Polym. Ed.* **1994**, *6*, 123.
(21) Harris, J. M., Ed. *Poly(ethylene glycol) Chemistry. Biotechnical and Biomedical Applications*; Plenum Press: New York, 1992.
(22) Glass, J. E., Ed. *Hydrophilic Polymers. Performance with Environmental Acceptance*; American Chemical Society: Washington DC, 1996.
(23) Prime, K. L.; Whiteside, G. M. *J. Am. Chem. Soc.* **1993**, *115*, 10714.
(24) Gombotz, W. R.; Guanghui, W.; Horbett, T. A.; Hoffman, A. S. *J. Biomed. Mater. Res.* **1991**, *25*, 1547.
(25) Lee, J.; Martic, P. A.; Tan, J. S. *J. Colloid Interface Sci.* **1989**, *131*, 252.
(26) Jeon, S. I.; Andrade, J. D.; de Gennes, P. G. *J. Colloid Interface Sci.* **1991**, *142*, 159.
(27) Roosjen, A.; van der Mei, H. C.; Busscher, H. J.; Norde, W. *Langmuir* **2004**, *20*, 10949.
(28) Uchida, K.; Otsuka, H.; Kaneko, M.; Kataoka, K.; Nagasaki, Y. *Anal. Chem.* **2005**, *77*, 1075.
(29) Otsuka, H.; Nagasaki, Y.; Kataoka, K. *Biomacromolecules* **2000**, *1*, 39.

Protein Adsorption Study. A protein adsorption study, which is an important reference for cell attachment, was performed using SPR equipment. Before the protein adsorption study, three types of PEGylated surface were constructed on a gold sensor chip in the same manner as described above: PEG5k(3), PEG5k(1)/2k(3), and PEG5k(2)/2k(4). And then protein adsorption was estimated by flowing 100 μL of serum-containing medium (EBM-2 medium to culture HUVEC) at a flow rate of 10 μL/min at 37 °C under running PBS (pH 7.4, 0.15 M) on the three types of PEGylated surface and native gold surface. The magnitude of the SPR angle shift by this injection was measured from the data taken from the final part of the curve after the surfaces were rinsed, and assessed as the amount of protein adsorbed. As a control, protein adsorption on a bare gold surface was examined.

2. Cell Culture Study. *Construction of PEGylated Surface.* Glass slides were etched with a boiling mixture of 50% (v/v) sulfuric acid and 50% (v/v) hydrogen peroxide for 30 min and then rinsed thoroughly with water. At 10^{-6} Torr, a 10 Å film of chromium was vapor-deposited at a rate of 0.1 Å/s onto the glass substrate. A 200 Å film of gold was then vapor-deposited on top of it at a rate of 0.1 Å/s. PEGylated surfaces were prepared on the gold films in the same manner as described for SPR measurements. PBS (pH 7.4, 0.15 M, containing 1 M NaCl) solutions of PEG5k (0.01 mg/mL) and PEG2k (0.01 mg/mL) were prepared. Then, PEG solutions with the appropriate conditions were retained on the gold film for 30 min to construct the PEGylated surfaces described above (PEG5k(3), PEG5k(1)/2k(3), PEG5k(2)/2k(4)). The plates were washed with Milli-Q water between each PEGylation, for 5 min each time.

Micropatterning of PEGylated Surface. The micropattern on the PEGylated surfaces were obtained by $N_2 + H_2$ plasma etching using a metal mask with holes 100 μm in diameter spaced 300 μm apart. After construction of a 2-well plastic chamber (Falcon BD) on the glass thus prepared, all samples were sterilized with ethylene oxide gas.

Cell Culture Study. HUVECs were seeded onto the micropatterned PEGylated surface at a cell density of 1×10^6 cells/mL. Cells were cultured at 37 °C in a humidified atmosphere of 5% CO_2. An EBM-2 medium was used for cultivation and was exchanged every 2 days.

Results and Discussion

Micropatterned PEGylated substrates with two-dimensional arrays of plasma-etched circular domains (ϕ = 100 μm) were prepared by sequential immobilization of PEG possessing a mercapto group at the end of the chain on the gold substrate, followed by plasma etching through a metal mask pattern with circular holes. The PEGylated region on the patterned substrate acts to repel proteins and thus inhibits cell adhesion. Proteins are expected to adsorb from the serum-containing medium onto the plasma-etched circular domains, exposing the base gold surface.

1. PEG Immobilization Study. The surface properties of the PEG coating were studied in detail to estimate protein adsorption and subsequent cell culture study on PEGylated surfaces. First, PBS solutions of various concentrations of PEG including 1 M NaCl were injected onto the gold surface using an SPR instrument to optimize immobilized concentration on a sensor chip. Use of high ionic strength buffer caused an increase in the amount of immobilized PEG, due to the appreciably reduced solubility of PEG in concentrated buffer solution.[30] The changes in SPR angle at each concentration of PEG5k are plotted in Figure 1. The results confirmed that the amount of immobilized PEG increased with increases in the injected PEG concentration; saturation was observed at PEG concentrations over 0.01 mg/mL, suggesting that the amount of possible immobilization on the gold surface is constant with injection of PEG above this concentration. There were no significant differences in this PEG immobilization study between PEG2k and PEG5k. Therefore, immobilization of PEG

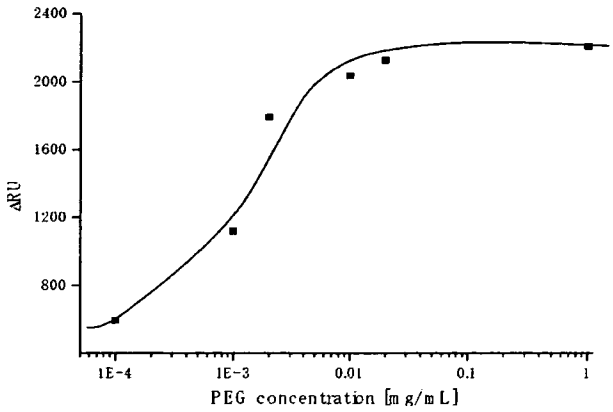

Figure 1. PEG immobilization as a function of PEG concentration. Flow rate, 10 μL/min; running buffer, PBS (pH 7.4, 0.15 M, containing 1 M NaCl); sample, PEG (M_w: 5k)/PBS (0.15 M, pH 7.4, containing 1 M NaCl) solution; sample injection, 100 μL.

on the gold surface was performed with 0.01 mg/mL PEG solution. Three types of PEG immobilization (PEG5k(3), PEG5k(1)/2k-(3), PEG5k(2)/2k(4), as described in the experimental section) were performed at this concentration, as shown in SPR sensorgrams (Figure 2). After first treatment with PEG5k, the sensor surface was washed under running buffer to remove noncovalently adsorbed PEG. The sensor chip was then treated again with a solution of PEG5k. This cycle of adsorption/rinsing of PEG5k was repeated several times. Eventually, the total SPR angle shift was amplified by increasing the number of treatment cycles to three, indicating that repetitive treatment with PEG5k was effective in increasing the density of PEG (PEG5k(3)). Notably, this trend became even more significant following additional treatment of the PEG5k surface with shorter PEG (PEG2k), as shown in Figure 2b,c. We planned to increase the surface brush density by PEG2k, retaining the PEG5k brush surface character. Sensorgrams showed a number of interesting findings. First, immobilization of long-chain PEG (PEG5k(1)) increased markedly with changes in SPR angle (Figure 2a–c). However, the extent of the shift decreased with the second injection of long-chain PEG (PEG5k(2)) (Figure 2a,c), and little change was seen on the third injection of long-chain PEG (PEG5k-(3)) (Figure 2a). On the other hand, immobilization of short-chain PEG (PEG2k(1)) after long-chain PEG resulted again in marked changes (Figure 2b,c). These results suggested that long-chain PEG5k can hardly penetrate into the preconstructed longer PEG-brushed layer due to its exclusion volume effect, while short-chain PEG2k appreciably filled the gap in the preconstructed longer PEG layer. It should be noted that SPR sensorgrams showed a steep increase curve in PEG2k(1), as shown in Figure 2b,c, indicating the importance of a short underbrushed PEG layer in increasing the PEG chain density.

To confirm that these SPR angle changes are reflected directly in the amount of immobilized PEG, QCM measurement was performed in the same manner as SPR (Table 1). The average value of total frequency shift after PEG injection is given as Δf in Table 1. PEG5k(2)/2k(4) surface showed the largest frequency shift, and PEG5k(1)/2k(3) surface also showed around 2000 Hz in frequency shift. On the other hand, PEG5k(3) surface showed around 1400 Hz in total frequency shift. Thus, PEG5k surface mixed with PEG2k showed larger mass change than only PEG5k chain immobilization, which suggested that more PEG chains were immobilized in PEG5k and PEG2k mixed surface. This result also indicated a significant role of a short underbrushed PEG layer in increasing the PEG chain density. On QCM

(30) Emoto, K.; Harris, J. M.; Alstine, M. V. *Anal. Chem.* **1996**, *68*, 3751.

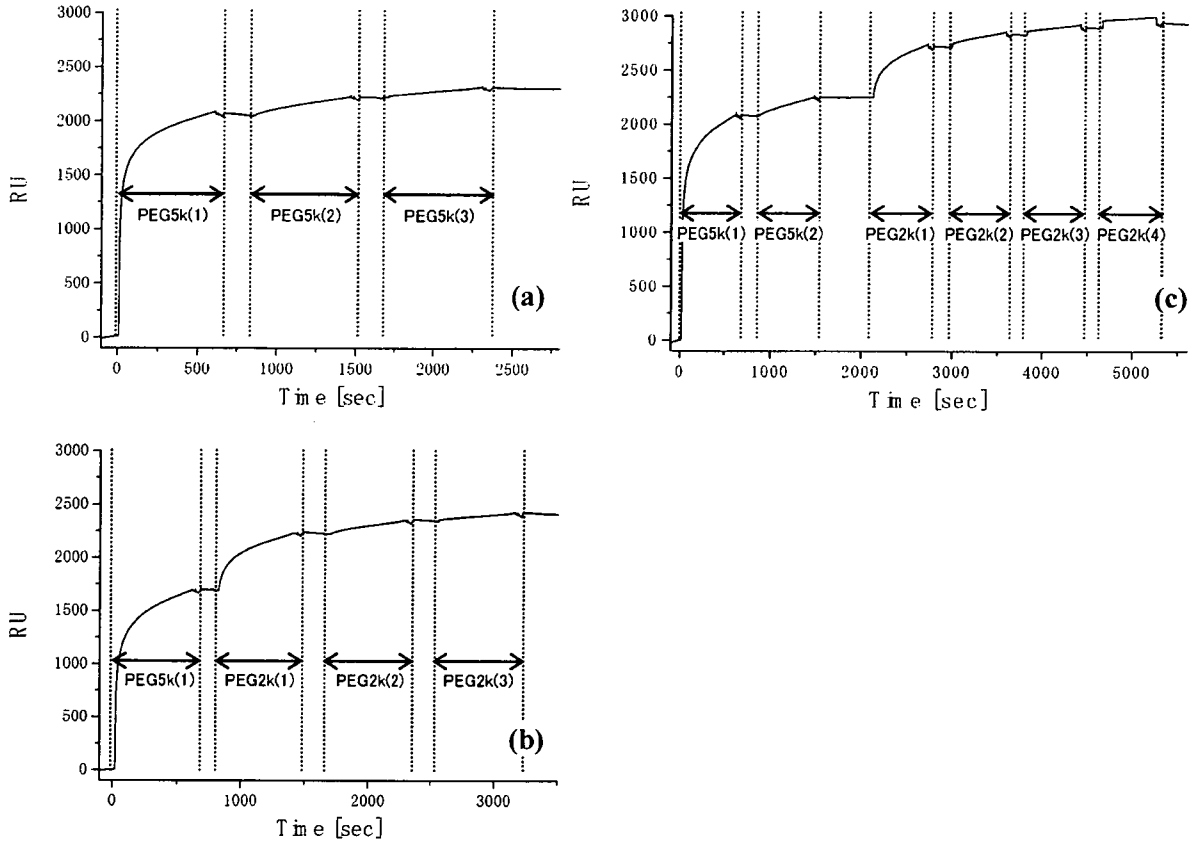

Figure 2. Sensorgrams of PEG immobilization on gold surfaces. (a) PEG5k(3), (b) PEG5k(1)/2k(3), and (c)PEG5k(2)/2k(4). Flow rate, 10 μL/min; running buffer, PBS (0.15 M, pH 7.4, containing 1 M NaCl); sample, 0.01 mg/mL of PEG (M_w: 5k or 2k)/PBS (0.15 M, pH7.4, containing 1 M NaCl) solution; sample injection, 100 μL for each time point.

Table 1. Comparison of Three Types of PEG Immobilization Measured by QCM: Δf is the Average of Total Frequency Shift after PEG Immobilization (n = 3)

PEG surfaces	Δf(Hz)	±S.D.
5k(3)	1382.8	118.6
5k(1)/2k(3)	1922.8	92.70
5k(2)/2k(4)	2144.7	81.74

measurement, the PEG5k(2)/2k(4) surface was determined to have the highest PEG chain density, while PEG5k(3) had the lowest.

The static wettability of the surface coated with PEG was estimated in both air and water by contact angle measurement (Figure 3). In the water-in-air measurement, the coating of PEG on the gold substrate significantly increased its wettability, as indicated by a decrease in the static contact angle (~30°). A similar trend was observed in the air-in-water measurement and the effect of PEG density on wettability was more pronounced, showing progressively increasing contact angle with increasing PEG chain density. Note that the increase in contact angle corresponds to an increase in wettability for the air-in-water system. As the accuracy of contact angle is ±2°, as shown by Zisman and co-worker,[31] significant differences could be seen between PEG surfaces. Furthermore, advancing/receding contact angles and hysteresis were measured on each PEG surface to estimate the dynamics of the uppermost surface in detail (Figure 4). In receding contact angles, each PEG surface showed a small value of around 15−20° and there was little difference between surfaces. On the other hand, critical differences were observed

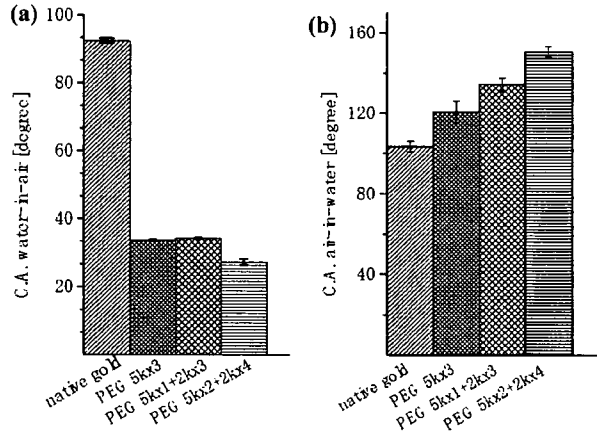

Figure 3. Static water contact angles on PEGylated gold surface. (a) Water-in-air system; (b) air-in-water system.

in advancing contact angles. PEG5k(3) and PEG5k(1)/2k(3) surfaces had around 30°, while the value for the PEG5k(2)/2k(4) surface was almost half. As PEG surfaces are easy to hydrate and show good water retentivity, once they became wet, receding contact angles showed small values in all PEG surfaces, resulting in little difference in receding contact angle. In contrast, significant differences were observed in advancing contact angles, indicating that the PEG5k(2)/2k(4) surface has the greatest wettability in the dry to wet state as compared with the other PEG surfaces examined. Hysteresis indicated differences between PEG5k(2)/2k(4) surfaces and the other surfaces according to its high surface free energy. When the water droplet extends, the surface with

(31) Fox, H. W.; Zisman, W. A. *J. Colloid Sci.* **1950**, *5*, 514.

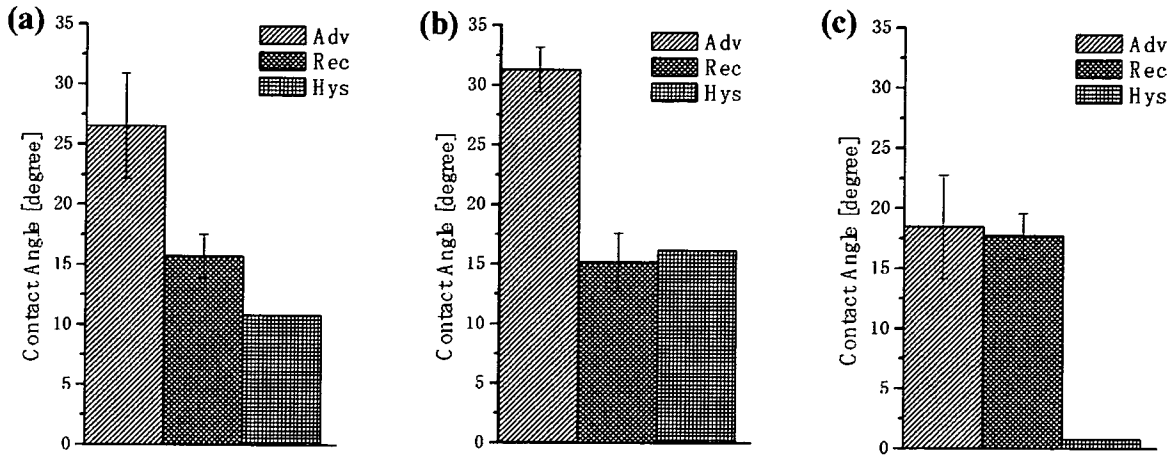

Figure 4. Dynamic water contact angles on PEGylated gold surfaces. (a) PEG5k(3), (b) PEG5k(1)/2k(3), and (c) PEG5k(2)2k(4).

a high surface free energy facilitates penetration of water, aiding in water droplet spreading, while the surface prevents the water droplet from receding when it contracts. Accordingly, the observations of the present study suggested that the PEG5k-(2)/2k(4) surface is the most hydrophilic and has a high surface free energy due to its high PEG chain density. Furthermore, the chain density is reported to have the relation with other parameters including the thickness and conformation of PEG layer.[23−27,32,33] The PEG chains (5k and 2k) are more well-oriented in this surface since the short, filler-like PEG2k chains will enhance the lateral interactions (e.g., hydrogen bonding and van der Waals force) between the PEG chains. This will likely result in much enhanced water affinity/penetration capability in PEG chains during the advancing angle measurement. Therefore, only small hysteresis value will be found on a PEG5k(2)/2k(4) surface.

Nonspecific protein adsorption from the culture medium for HUVEC was estimated on each PEG-coated surface to estimate the cytophobicity of PEGylated surfaces because the adsorbed proteins are responsible for subsequent cell adhesion. On bare gold as a control, the SPR angle shift due to the nonspecific adsorption of protein was 2927.4 RU, when a serum-containing cell (HUVEC) culture medium (EBM-2) was passed over the surface for 10 min at a flow rate of 10 μL/min. In contrast, PEG-coated surfaces clearly reduced protein adsorption (Figure 5). Figure 5 also shows a comparison of protein adsorption on the three types of PEG surface. The SPR angle shift was 676.5, 350.8, and 218.0 RU on PEG5k(3), PEG5k(1)/2k(3), and PEG 5k(2)/2k(4) surfaces, respectively. The PEG5k(2)/2k(4) surface showed the greatest degree of inhibition of protein adsorption from the medium, suggesting that the inhibitory effect of nonspecific protein adsorption was the highest for this surface among those studied. The physicochemical properties of PEG surfaces described above indicate that PEG surfaces with higher immobilized PEG chain density have greater ability to repel proteins. Based on these results, it was concluded that shorter PEG, viz. an underbrushed layer to increase the PEG surface density, played a substantial role in minimizing nonspecific protein adsorption. Other workers have also proposed that PEG mixtures, which are polydisperse with respect to molecular weight, are more efficacious than single molecular weights. Mixed PEGs were shown to have greatest efficacy in steric stabilization of colloidal particles and in protein repellency.[34,35] The PEG5k-

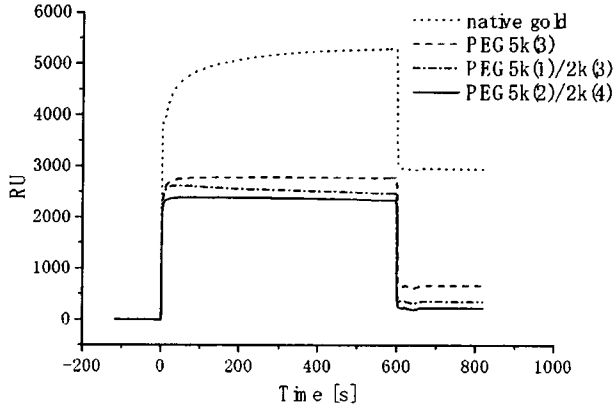

Figure 5. Sensorgrams of injection of serum-containing cell culture medium (EBM-2 medium to culture HUVEC) on native gold and each PEGylated surfaces. Flow rate, 10 μL/min; running buffer, PBS (pH 7.4, 0.15 M); sample injection volume, 100 μL.

(2)/2k(4) surface with the highest PEG chain density was expected to have the highest cytophobicity.

2. Cell Culture Study. Gold surfaces were coated with PEG to inhibit nonspecific protein adsorption and were expected to act as cytophobic surfaces for subsequent cell patterning. The PEG-coated gold substrates were micropatterned by plasma etching ($N_2 + H_2$) through a metal mask pattern with ϕ100 μm circular holes separated by 300 μm (edge-to-edge distance), and cell culture dishes were then set onto these surfaces (2 × 2 cm). Microscopic images following seeding of HUVEC on the surfaces are shown in Figure 6. On PEG5k(3) surfaces with lower PEG chain density as suggested by physicochemical studies, seeded HUVEC showed disorganized cellular attachment regardless of micropatterned substrate (Figure 6a). On the other hand, the PEG5k(1)/2k(3) surface (Figure 6b) and PEG5k(2)/2k(4) surface (Figure 6c) showed patterned cell attachment due to the suggested higher PEG chain density compared with that of the PEG5k(3) surface, although cells that had overgrown beyond the pattern were still observed on PEG5k(1)/2k(3) surfaces. The results of cultivation of HUVECs for 1 week are shown in Figure 6d−f. Arrayed cellular attachment was observed only on the PEG5k-(2)/2k(4) surface (Figure 6f). In contrast, the HUVECs began to bridge across multiple islands on the PEG5k(1)/2k(3) surface (Figure 6e) and this bridging was more pronounced to form a complete cell sheet on the PEG5k(3) surface (Figure 6d). It is

(32) Harder, P.; Grunze, M.; Dahint, R.; Whitesides, G. M.; Laibinis, P. E. *J. Phys. Chem.* **1998**, *102*, 426.
(33) Zhu, B.; Eurell, T.; Gunawan, R.; Leckband, D. *J. Biomed. Mater. Res.* **2001**, *56*, 406.
(34) Stenkamp, V. S.; Berg, J. C. *Langmuir* **1997**, *13*, 3827.
(35) Pavey, K. D.; Olliff, C. J. *Biomaterials* **1999**, *20*, 885.

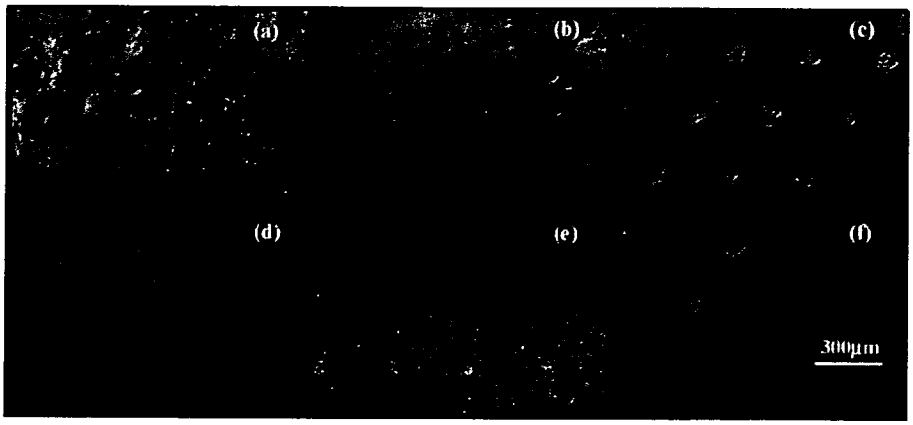

Figure 6. Microscopic image of cell seeding study. After 1 day of culture of HUVEC on micropatterned (a) PEG5k(3) surface, (b) PEG5k(1)/2k(3) surface, and (c) PEG5k(2)/2k(4) surface. After 1 week of culture of HUVEC on micropatterned (d) PEG5k(3) surface, (e) PEG5k(1)/2k(3) surface, and (f) PEG5k(2)/2k(4) surface.

clear that PEG chain density affects pattern recognition in cell attachment. The threshold density for HUVEC bridging seems to exist on the surface between PEG5k(3) and PEG5k(2)/2k(4). Cells overgrew beyond the pattern on weak protein-repellent surfaces. In addition, when overgrown cells grew sufficiently close together, bridging occurred between overgrown cellular patterns. Attached patterns eventually resulted in sheet formation. As described above, no pattern recognition of cell attachment was seen on the surfaces coated only with long-chain PEG (PEG5k(3)) because of its lower inhibitory effect on nonspecific protein adsorption. In contrast, cell array formation was observed by constructing long- and short-chain PEG mixed surfaces. Furthermore, PEG5k(2)/2k(4) surfaces showed the least nonspecific cell attachment in contrast to some nonspecific cell attachment and bridging of cellular islands on PEG5k(1)/2k(3) surfaces. SPR results indicated that cell-adhesive proteins are greatly repelled on PEG5k(2)/2k(4) surfaces to promote pattern recognition of cell attachment. Some cell attachment between cellular islands was confirmed on PEG5k(3) and 5k(1)/2k(3) surfaces after 1 day in culture, and the attached cells extended toward each other and bridging occurred across cellular islands. Bridged cellular patterns grew everywhere on the surface and eventually formed a complete cell sheet. As the first cell attachment on the cytophobic region depends on the ability of the surface to repel protein, surfaces with lower PEG chain density (PEG5k(3) or PEG5k(1)/2k(3)) resulted in cell attachment and cell sheet formation. Thus, the results of the cell culture study agreed well with the surface properties, suggesting that PEG chain density played a critical role in micropatterned cell attachment.

Conclusions

To gain insight into the design of cellular microenvironments, we examined the micropatterning of endothelial cells on microfabricated gold substrates coated with PEG brushes in terms of the relationship between PEG chain density and cellular attachment. A PEG-brushed layer was constructed on a gold substrate using PEG with a mercapto group at the chain end. After treatment with longer chain PEG with a molecular weight of 5000, shorter chain PEG (2000) was introduced onto the gold substrate to modulate the chain density. In this way, PEGylated surfaces with different chain densities were produced, and subsequent micropatterning was achieved by plasma etching through a micropatterned metal mask. The results indicated that cell pattern formation was strongly dependent on both the PEG chain density and the extent of protein adsorption, as evidenced by physicochemical and biological characterization of PEGylated surfaces using SPR, QCM, and static/dynamic contact angle measurements. Cell micropatterning showed long-term retention only on the surfaces with greater disparity between cytophobic and cytophilic regions. Notably, a PEG chain density sufficiently high to inhibit outgrowth of endothelial cells beyond the cytophilic gold region to the cytophobic PEGylated region could be obtained only on the mixed PEG chain-tethered surface, which achieved almost complete prevention of nonspecific protein adsorption. These observations clearly indicated that shorter PEG, viz. an underbrushed PEG layer to increase the PEG surface density, played a substantial role in minimizing nonspecific protein adsorption and long-term maintenance of the active cell pattern. It should be noted that the precise control of surface properties in single-molecule order directly affected micropatterned cellular attachment. Therefore, we envision the cellular micropatterning technique presented here becoming a valuable tool for the control of cell−surface and cell−cell interactions on a micrometer scale and to evaluate local effects of engineered microenvironments on cellular behavior. The surface fabrication technique studied here is a promising technology for the development of tissue/cell-based biosensors and in the field of tissue engineering.

Acknowledgment. Microfabrication using the plasma etching technique was conducted at the National Institute for Materials Science (NIMS), Japan, with assistance from Dr. Y. Horiike. Financial support for this work was partly provided by Special Coordination Funds for Promoting Science and Technology and also supported by Research Promotion Bureau under contract nos. 15-99 and 15-396, both from the Ministry of Education, Culture, Sports, Science, and Technology (MEXT), Japan. Part of this work was also supported financially by a Grant-in-Aid for Research on Health Sciences for Drug Innovation (KH71066), Ministry of Health, Labor, and Welfare of Japan, and The New Energy and Industrial Technology Development Organization (NEDO).

LA0624384

Bone Regeneration by Regulated *In Vivo* Gene Transfer Using Biocompatible Polyplex Nanomicelles

Keiji Itaka[1], Shinsuke Ohba[1], Kanjiro Miyata[2], Hiroshi Kawaguchi[3], Kozo Nakamura[3], Tsuyoshi Takato[3], Ung-Il Chung[1] and Kazunori Kataoka[1,2]

[1]*Division of Clinical Biotechnology, Center for Disease Biology and Integrative Medicine, Graduate School of Medicine, The University of Tokyo, Tokyo, Japan;* [2]*Department of Materials Science and Engineering, Graduate School of Engineering, The University of Tokyo, Tokyo, Japan;* [3]*Division of Sensory and Motor System Medicine, Faculty of Medicine, The University of Tokyo, Tokyo, Japan*

Gene therapy is a promising strategy for bone regenerative medicine. Although viral vectors have been intensively studied for delivery of osteogenic factors, the immune response inevitably inhibits bone formation. Thus, safe and efficient non-viral gene delivery systems are in high demand. Toward this end, we developed a polyplex nanomicelle system composed of poly(ethyleneglycol) (PEG)-block-catiomer (PEG-b-P[Asp-(DET)]) and plasmid DNA (pDNA). This system showed little cytotoxicity and excellent transfection efficiency to primary cells. By the transfection of constitutively active form of activin receptor-like kinase 6 (caALK6) and runt-related transcription factor 2 (Runx2), the osteogenic differentiation was induced on mouse calvarial cells to a greater extent than when poly(ethylenimine) (PEI) or FuGENE6 were used; this result was due to low cytotoxicity and a sustained gene expression profile. After incorporation into the calcium phosphate cement scaffold, the polyplex nanomicelles were successfully released from the scaffold and transfected surrounding cells. Finally, this system was applied to *in vivo* gene transfer for a bone defect model in a mouse skull bone. By delivering *caALK6* and *Runx2* genes from nanomicelles incorporated into the scaffold, substantial bone formation covering the entire lower surface of the implant was induced with no sign of inflammation at 4 weeks. These results demonstrate the first success in *in vivo* gene transfer with therapeutic potential using polyplex nanomicelles.

Received 31 December 2006; accepted 30 April 2007; published online 5 June 2007. doi:10.1038/sj.mt.6300218

INTRODUCTION

Despite bone's capacity to heal spontaneously, bone repair is not always satisfactory. Approximately 5–10% of fractures do not heal well, resulting in delayed union or non-union with considerable morbidity.[1] Critical bone defects after severe trauma, tumor resection, or revision of total joint arthroplasty remain challenging problems. Autologous bone graft is considered the gold standard technique; however, it has shortcomings concerning both quantity (availability of material) and quality (donor site troubles, graft rejection, disease transmission).[2,3] These problems have heightened the need for bone regenerative medicine that uses tissue engineering techniques.[4]

A promising strategy is to combine adequate scaffolds and signals. Although some scaffolds are osteoconductive, no scaffolds invented so far are known to be osteoinductive,[5] because current scaffold materials cannot activate the signals necessary for osteogenesis. For this purpose, the potential of growth and transcriptional factors has been widely recognized.[6,7] Substantial progress has been made in the basic understanding of major osteogenic signaling molecules such as bone morphogenetic proteins (BMPs),[8] Hedgehogs,[9] Runx2,[10] Wnts,[11] and insulin-like growth factors.[12] In particular, recombinant human BMP-2 and BMP-7 have already been approved by the U.S. Food and Drug Administration for restricted clinical use. However, in spite of the remarkable findings on animal studies, clinical trials using BMP devices have not obtained comparable outcomes.[13,14] Problems such as protein stability, inadequate release profile (initial burst effect), or the need for accessory factors may have caused these inconsistent results.[6,15]

Gene therapy is a promising approach to overcome these problems. Compared with exogenous proteins, which require purification, the gene can express these bioactive factors in the native form at the regeneration site.[6] The sustained synthesis of proteins from the delivered gene can facilitate synchronization between the kinetics of signaling receptor expression and bioactive factor availability.[16] In addition, the combined use of two or more osteoinductive factors to constitute a better osteogenic signal can be evaluated with a high degree of flexibility.[17] For this purpose, viral vectors including adenovirus and adeno-associated virus vectors have been intensively studied for the delivery of the osteoinductive cytokines.[17–21] However, when these viral vectors are used, there is concern about inducing immune responses.[22] Indeed, Egermann *et al.* reported that, after a local injection of BMP-2 expressing adenoviral vector to a bone defect area in sheep, bone formation was significantly reduced even at the untreated contralateral defect area, indicating that the immune

The first two authors contributed equally to this work.

Correspondence: *Kazunori Kataoka, Department of Materials Science and Engineering, Graduate School of Engineering, The University of Tokyo, 7-3-1 Hongo, Bunkyo-ku, Tokyo 113-0033, Japan. E-mail: kataoka@bmw.t.u-tokyo.ac.jp*

response has a systemic inhibitory effect on bone formation after a single injection of adenovirus.[23]

In this context, safe and efficient non-viral gene delivery systems are in high demand. We recently developed a novel polymer-based gene delivery system that showed excellent capacity for *in vitro* transfection.[24] This system is a polyplex nanomicelle composed of poly(ethyleneglycol) (PEG)-block-polycation (PEG-b-P[Asp-(DET)]): PEG-b-polyasparagine carrying the *N*-(2-aminoethyl)aminoethyl group $(CH_2)_2NH(CH_2)_2NH_2$ as the side chain) and plasmid DNA (pDNA). The complexation of block copolymer and pDNA forms a micellar structure, and its characteristics have been found suitable for gene delivery: a diameter of ~100 nm with a PEG palisade enabling complexes to avoid foreign body recognition while providing increased nuclease resistance, increased tolerance under physiologic conditions, and excellent gene expression in a serum-containing medium.[25–27] In addition, the cationic segment of block copolymer was designed to have the buffering capacity of an acidic environment inside the endosomes as effected by the presence of unprotonated amines under neutral pH. By virtue of these features, we effectively transfected genes to culture cells with almost no cytotoxicity.[24]

We undertook the present study to investigate the feasibility of these polyplex nanomicelles for bone regenerative medicine, including the study of: (i) transfection toward various primary cells for the evaluation of efficiency and safety, (ii) induction of osteogenic differentiation by a foreign gene introduction of osteogenic factors, and (iii) *in vivo* gene transfer to a mouse bone defect model to increase the rate of bone regeneration. As will be shown, this system provides sufficient gene expression in a sustained manner both *in vitro* and *in vivo*, and it thus shows a potential therapeutic effect in a bone defect model.

RESULTS

In vitro transfection to human synovial cells

To evaluate the feasibility of polyplex nanomicelles for clinical gene therapy, *in vitro* transfection was performed toward human synovial cells derived from patients suffering from rheumatoid arthritis. By evaluating luciferase gene expression on day 2 of transfection, the polyplex nanomicelles that were formed at an optimal nitrogen/phosphate ratio showed gene expressions comparable to those of linear poly(ethylenimine) (LPEI),[28] which is well known to have excellent transfection efficiency (**Figure 1a**). At the optimal nitrogen/phosphate = 80, the polyplex nanomicelles were observed to have small absolute zeta potentials of around +10 mV (**Supplementary Figure S1**). The nanomicelles maintained appreciable gene expression even on day 5, whereas the gene expression of LPEI showed a marked decrease during the same time frame. To investigate this difference, the cytotoxicity was evaluated by a quantitative assay. Consistent with the results of gene expression, LPEI exhibited prominent cytotoxicity time-dependently (**Figure 1b**). The microscopic images following green fluorescence protein (GFP) gene transfection by LPEI showed apparent morphologic change as well as reduced numbers of cells, whereas the polyplex nanomicelles maintained almost normal phenotype concurrently with GFP expression even on day 5 (**Supplementary Figure S2**). Thus, the polyplex

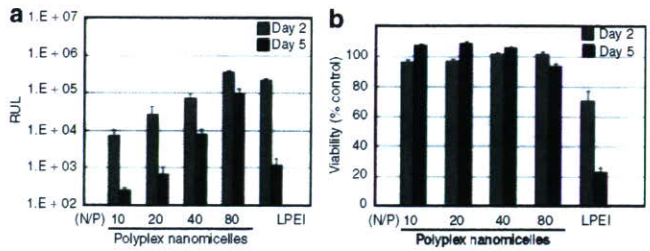

Figure 1 *In vitro* transfection to human synovial cells. (**a**) Luciferase gene expression. *In vitro* transfection of luciferase-expressing plasmid DNA was performed by polyplex nanomicelles formed at various nitrogen/phosphate (N/P) ratios and by poly(ethylenimine) (LPEI). Gene expression was evaluated after 2 and 5 days of transfection. Data are means ± SDs, $n = 4$. (**b**) Cell viability after transfection. After transfection, similar to the case in **a**, cell viability was estimated by an MTT assay. Results were expressed as the relative value (%) of the control cells, which were incubated in parallel without transfection. Data are means ± SDs, $n = 8$. RLU, relative light units.

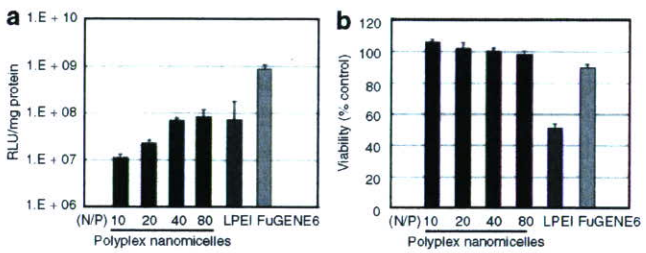

Figure 2 *In vitro* transfection to mouse calvarial cells. (**a**) Luciferase gene expression. *In vitro* transfection of luciferase-expressing plasmid DNA was performed using polyplex nanomicelles, formed at various nitrogen/phosphate (N/P) ratios, as well as poly(ethylenimine) (LPEI) and FuGENE6. Gene expression was evaluated after 2 days of transfection. Data are means ± SDs, $n = 4$. (**b**) Cell viability after transfection. After transfection, similar to the case in **a**, cell viability was estimated by an MTT assay. Results were expressed as relative values (%) of the control cells, which were incubated in parallel without transfection. Data are means ± SDs, $n = 8$. RLU, relative light units.

nanomicelles were revealed to have excellent gene transfection capacity—comparable to that of LPEI—with considerably low cytotoxicity; this suggests a great advantage for *in vivo* application.

Transfection toward mouse calvarial cells and induction of osteogenic differentiation

In applying polyplex nanomicelles to delivery genes encoding bioactive factors that activate signals necessary for osteogenesis, we evaluated the transfection capacity of foreign genes and the induction of cell differentiation toward mouse calvarial cells derived from neonatal calvariae. The evaluation of luciferase showed that gene expressions comparable to those of LPEI were obtained by polyplex nanomicelles (**Figure 2a**) without showing any cytotoxicity (**Figure 2b**). From a practical standpoint we also evaluated FuGENE6, a commercially available lipid-based transfection reagent with considerably high efficiency and biocompatibility.[29–33] With this reagent, the cells showed luciferase expression that was one order higher than with polyplex nanomicelles or LPEI and with little cytotoxicity (**Figure 2a** and **b**).

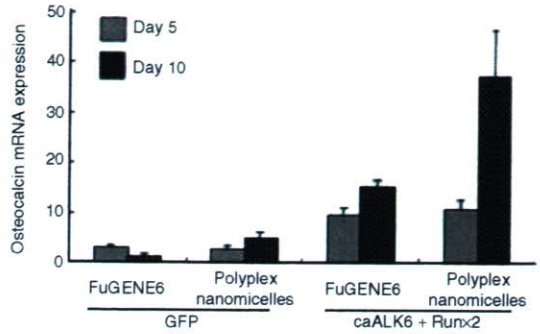

Figure 3 Evaluation of osteocalcin messenger RNA (mRNA) expression by a quantitative polymerase chain reaction (PCR). Osteogenic differentiation was induced on the mouse calvarial cells by transfection of caALK6 and Runx2 expressing plasmid DNAs. As a negative control, a green fluorescence protein (GFP) gene was also used. After 5 and 10 days, the total RNA was collected and the osteocalcin expression was quantified by a quantitative PCR. Data are means ± SDs, $n = 6$. caALK6, constitutively active form of activin receptor-like kinase 6; Runx2, runt-related transcription factor 2.

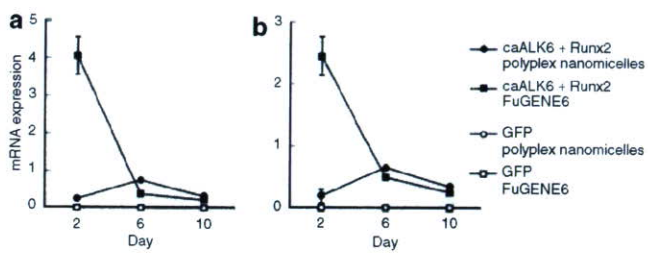

Figure 4 Evaluation of messenger RNA (mRNA) expression of (a) constitutively active form of activin receptor-like kinase 6 (caALK6) and (b) runt related transcription factor 2 (Runx2) after transfection by a quantitative polymerase chain reaction. Two, six and ten days after transfection, the mRNA expression of ALK6 and Runx2 was quantified. Data are means ± SDs, $n = 6$. caALK6, constitutively active form of activin receptor-like kinase 6; GFP, green fluorescence protein; Runx2, runt-related transcription factor 2.

Observation of GFP expression revealed that nanomicelles and FuGENE6 achieved similar levels of gene expression without showing any morphologic changes in the cells; this is evident in the phase contrast images (**Supplementary Figure S3**).

We then investigated the osteogenic differentiation after transfection of pDNAs expressing a constitutively active form of activin receptor-like kinase 6 (caALK6) and runt-related transcription factor 2 (Runx2), which have been shown to be a potent combination of genes for bone regeneration.[34] Osteogenic differentiation was evaluated by the expression of osteocalcin messenger RNA (mRNA), an osteoblast-differentiation marker. As shown in **Figure 3**, the time-dependent increase in osteocalcin expression was confirmed after transfection of caALK6 + Runx2 by both polyplex nanomicelles and FuGENE6. Using LPEI, in contrast, osteocalcin expression was at the same level as the control cells transfected with the GFP gene (data not shown). It is interesting that, on day 10, nanomicelles showed a more remarkable increase in osteocalcin expression than did FuGENE6, although both showed comparable gene expression without cytotoxicity by the luciferase and GFP reporter assays (**Figure 2a** and **b** and

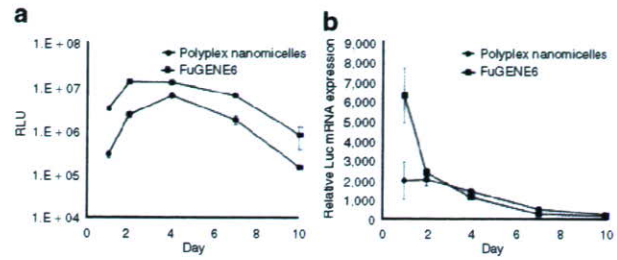

Figure 5 Evaluation of sustained expression of luciferase on mouse calvarial cells. (**a**) Luciferase expression measured by luminescence, which indicated the quantification of protein synthesis. Data are means ± SDs, $n = 12$. (**b**) Estimation of the corresponding messenger RNA (mRNA) expression by a quantitative polymerase chain reaction. For both, the mouse calvarial cells were transfected by luciferase-expressing plasmid DNA and the assays were done on days 1, 2, 4, 7, and 10. Data are means ± SDs, $n = 6$. RLU, relative light units.

Supplementary Figure S3). It is reasonable to assume that, with the same transfection procedure as used with the reporter genes, *caALK6* and *Runx2* were also expressed similarly by nanomicelles and FuGENE6. The reasons for this disparity in osteocalcin induction are unclear, but FuGENE6 may cause some appendant effect on cell differentiation that is difficult to detect by a nonspecific viability evaluation such as the MTT assay.[35] Regarding this concern we speculated that, since the difference was visible on day 10, the expression profile of the transfected genes might differ between nanomicelles and FuGENE6, thus affecting the outcome of the induction of cell differentiation.

To investigate this possibility, the time-dependent change of gene expression was quantified. As shown in **Figure 4**, the mRNA expressions of caALK6 and Runx2 showed similar profiles, where FuGENE6 initially induced expressions of ALK6 and Runx2 that were one order higher than nanomicelles, although the expressions sharply decreased with time. In contrast, the nanomicelles showed rather consistent gene expressions. For a detailed investigation, the luciferase gene was used and the protein systhesis and its mRNA expression were simultaneously quantified by a luminescence measurement and a quantitative polymerase chain reaction (PCR), respectively. As shown in **Figure 5**, FuGENE6 initially showed light emission (indicating the amount of synthesized protein) that was one order higher than did the nanomicelles. The highest expression was obtained on day 2. The initial mRNA expression was always high, but a rapid decrease was observed after day 2. In contrast, the polyplex nanomicelles showed fairly consistent gene expression profiles, giving the highest luciferase expression on day 4 and with sustained mRNA expression thereafter. Because cell differentiation would require some processes in signaling pathways inside the cells, it follows that such a continuous manner of gene expression by polyplex nanomicelles might contribute to the efficient induction of differentiation. Hence, the nanomicelle profile is a promising feature for *in vivo* bone regeneration.

In vitro transfection from gene-containing scaffolds

The *in vivo* gene transfer to a bone regeneration site should require the retention and gradual release of gene carriers. One promising approach is to incorporate the carriers into implantable scaffolds.

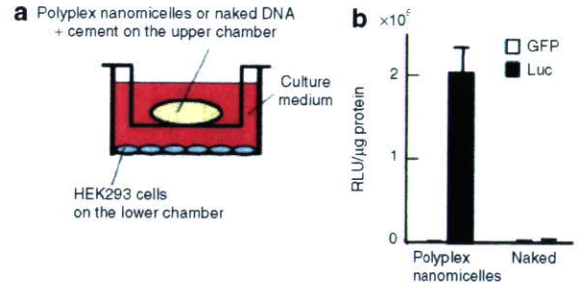

Figure 6 *In vitro* transfection by polyplex nanomicelles incorporated into calcium phosphate cement scaffold. (**a**) Schematic illustration of the *in vitro* transfection from the gene-containing scaffolds. The scaffold containing polyplex nanomicelles of PEG-b-P[Asp-(DET)] and plasmid DNA (pDNA) expressing luciferase gene or naked pDNA was plated onto the upper chamber of cell culture insert, and the HEK293 cells were plated onto the lower chamber. (**b**) Luciferase expression in HEK293 cells. After 5 days of transfection, luciferase expression was measured. The green fluorescence protein (GFP) gene was used as a negative control. Data are means ± SDs, $n = 3$. DET, diethylenetriamine; PEG, poly(ethyleneglycol); RLU, relative light units.

This form of gene delivery is called the gene-activated matrix, through which Bonadio *et al.* pioneered the incorporation of non-viral vectors in collagen scaffolds to stimulate bone formation in a rat defect model.[36] In this study, the polyplex nanomicelles were incorporated into a calcium phosphate cement scaffold by mixing. This process is highly biocompatible, bioactive (especially in bone tissue), moldable, and injectable.

In order to investigate whether or not the polyplex nanomicelles containing luciferase-expressing pDNA were delivered from the calcium phosphate cement scaffold, the scaffold was put into the culture medium of HEK293 cells for 5 days. The cement and the cells were physically separated by a filter to avoid direct contact between the cement and the cells, which could hinder the distinction between the release and the direct delivery of polyplex nanomicelles from the scaffold (**Figure 6**). As shown in **Figure 6b**, the cells cultured with the scaffold containing the polyplex nanomicelles exhibited apparent luciferase expression, whereas the cells cultured with the scaffold containing naked pDNA did not. Thus, the polyplex nanomicelles incorporated into the calcium phosphate cement scaffold successfully introduced the contained genes into the surrounding cells.

Next, to investigate how long the transfection by polyplex nanomicelles incorporated into the scaffold would last, the scaffold was placed on the culture dish and then mouse calvarial cells were plated on top of it and cultured for an extended period. Monitoring of luminescence using the IVIS Imaging System (Xenogen, Alameda, CA) revealed that the gene expression of mouse calvarial cells by the scaffold containing polyplex nanomicelles with luciferase-expressing pDNA increased, peaking near days 10 and 18, and then gradually declined to the background level approaching day 25 (**Supplementary Figure S4a**). Quantitative visualization of luminescence using this imaging system revealed that cells on top of the scaffold and in its close proximity were first transfected at days 2 and 10; subsequently, cells at some distance were transfected until day 25 (**Supplementary Figure S4b**). Thus, the polyplex nanomicelles incorporated into the scaffold delivered genes in a sustained manner.

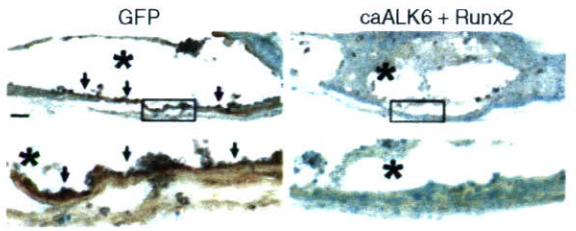

Figure 7 *In vivo* gene transfer by polyplex nanomicelles. Immunohistochemistry for green fluorescence protein (GFP) of calvarias implanted with the scaffold containing polyplex nanomicelles of PEG-b-P[Asp-(DET)] and plasmid DNA expressing GFP or caALK6 + Runx2 at 4 weeks after implantation. GFP protein was stained brown (arrows). The lower panel of each group shows a magnified view of the boxed area in the upper panel. Asterisks denote the remnants of calcium phosphate pastes. Scale bar: 200 μm. caALK6, constitutively active form of activin receptor-like kinase 6; DET, diethylenetriamine; PEG, poly(ethyleneglycol); Runx2, runt-related transcription factor 2.

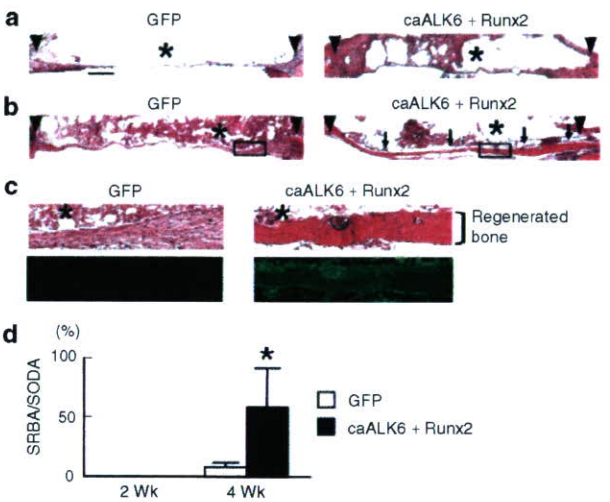

Figure 8 Bone regeneration by polyplex nanomicelles. (**a**, **b**) Histologic analyses of calvarias. The scaffold containing polyplex nanomicelles of PEG-b-P[Asp-(DET)] and plasmid DNA expressing green fluorescence protein (GFP) or caALK6 + Runx2 was implanted on the bone defect area on the mouse skull bone. At (**a**) 2 weeks and (**b**) 4 weeks after implantation, histologic and immunohistologic analyses were performed. Sections were stained with hematoxylin and eosin (H&E). Arrowheads denote defect edges; arrows, regenerated bones; asterisks, the remnants of calcium phosphate cement. Scale bar: 500 μm. (**c**) Magnified views of boxed areas in **b**. H&E (bright field views) and immunohistochemstry for type-I collagen (dark field views) were performed on serial sections. Green fluorescence indicates expression of type-I collagen. Asterisks, the remnants of calcium phosphate cement. (**d**) Quantification of bone regeneration. The ratio of the summation of the regenerated bone area to that of the original defect area (SRBA/SODA) in designated sections was histologically measured by NIH Image software. Data are means ± SD of five mice per group. *$P < 0.01$ versus GFP at 4 weeks after implantation. caALK6, constitutively active form of activin receptor-like kinase 6; DET, diethylenetriamine; PEG, poly(ethyleneglycol); Runx2, runt-related transcription factor 2.

In vivo gene delivery to the bone defect area on the mouse calvarial bone

The data so far have shown that a localized and sustained system to deliver polyplex nanomicelles was successfully developed *in vitro* using the calcium phosphate cement scaffold. To

investigate whether or not this system is effective for *in vivo* gene delivery, the scaffold was molded to the fitting shape and implanted in mouse calvarial bone defects. After implantation of the scaffold containing polyplex nanomicelles with GFP pDNA, successfully transfected recipient cells were observed across a few layers from the implant surface by immunohistochemical analyses (**Figure 7**). The intensity of the staining was strongest in cells immediately adjacent to the scaffold, gradually declining with distance.

To investigate the therapeutic potential of this system, polyplex nanomicelles containing pDNAs expressing a caALK6 and Runx2, by which the osteogenic differentiation was induced on the calvarial cells *in vitro* (**Figure 3**), were incorporated into the calcium phosphate cement scaffold and implanted in the same model. At 2 weeks after implantation, no bone formation occurred in either the control group transfected with the GFP-expressing pDNA or the treatment group transfected with caALK6 + Runx2 expressing pDNA (**Figure 8a**). At 4 weeks after implantation, however, substantial bone formation covering the entire lower surface of the implant was induced only in the treatment group (**Figure 8b**), as confirmed by the quantitative analysis of the regenerated bone area (**Figure 8d**). The regenerated bone tissues exhibited a lamellar structure containing osteocyte-like cells and strongly expressed the type-I collagen protein (**Figure 8c**). On the other hand, the incorporation of neither the LPEI nor the FuGENE6 complex into the calcium phosphate cement scaffold generated any apparent bone formation at 4 weeks (data not shown). It should be noted that no sign of inflammation was observed in any group (**Figure 8a–c**). The results so far indicate that the polyplex nanomicelles incorporated into the calcium phosphate cement scaffold transfected the foreign genes to the cells in the vicinity of the scaffold, leading to a considerable increase in the rate of bone formation via the induction of osteogenic differentiation.

DISCUSSION

Many clinical fields demand useful non-viral gene delivery systems that satisfy high standards of both efficacy of gene introduction and low toxicity.[37] Bone tissue engineering would be a promising field; however, only a few trials have been reported so far. Bright *et al.* used a naked pDNA expressing OP-1 (BMP-7) gene, which was incorporated into a collagen scaffold, for a rat model of lumbar interbody arthrodesis.[38] Although bone formation was stimulated after 4 weeks, it was not as extensive as that observed after the injection of recombinant human OP-1 protein, in spite of considerably high dose of pDNA (250 μg/rat). Huang *et al.* combined poly(lactic-co-glycolic acid) scaffolds with 200 μg of condensed pDNA encoding BMP4 using branched PEI and implanted the scaffolds into rat cranial defects.[39] They successfully induced bone regeneration at the defect edges; however, osteoid and mineralized tissue was significantly increased after 15 weeks of implantation. The disparity between our results and theirs presumably resulted from the difference in the osteogenic signals. However, some toxic effects of PEI should also be taken into consideration: PEI was reported to be an apoptotic agent,[40] and indeed in our results it showed appreciable cytotoxicity (**Figures 1b** and **2b**) and an inability to induce differentiation. Directly comparing the capacity of their versus our method was not possible because Huang *et al.* did not provide data on the actual transfection efficiency; however, some negative effects of PEI on the cells in the vicinity of the scaffold may have caused the delayed induction of bone regeneration.

The considerably low dose of pDNA (1.3 μg/mouse) is also characteristic in our system. In previous studies of *in vivo* bone formation by non-viral gene delivery systems, a larger amount of pDNA (100 μg to 1 mg) was used.[38,39,41] We assume that this may be attributed to the capacity of polyplex nanomicelles to stably retain pDNA even in the scaffolds. Moreover, using the combination of osteogenic genes *caALK6* and *Runx2* contributed to the efficient osteoconductivity of our system. The cooperative action of this combination occurred through protein stabilization of core binding factor beta (Cbfb) and through induction of Runx2–Cbfb complex formation and its DNA binding, leading to the efficient induction of osteogenic differentiation.[34]

FuGENE6 has often been reported to have excellent transfection efficiency *in vitro*, including the induction of cell differentiation.[29–33] Indeed, in our results shown in **Figure 3**, comparable induction of osteocalcin expression was observed by both FuGENE6 and polyplex nanomicelles on day 5. It is interesting to note that, although the gene expressions evaluated by luciferase were consistently higher in FuGENE6 until day 10 (**Figure 5**), the osteocalcin induction was more remarkable in the nanomicelles on day 10 (**Figure 3**). The marked difference in gene expression profiles between nanomicelles and FuGENE6—especially when evaluated by mRNA expression—might influence the outcome of cell differentiation, which requires complex intracellular processes over an extended period. It is also possible that some toxicologic effects of the reagents might influence the cell reactivity, since many lipid-based transfection reagents were reported to induce changes in the expression of endogenous genes.[42] The study of toxicologic or pharmacologic effects of bioactive materials that might alter responses to delivered drugs or genes is now attracting attention as polymer (material) genomics.[43] From this standpoint, we have started comprehensive analyses of cell bioactivities after various transfection procedures, including the study of endogenous gene expression profiles using complementary DNA arrays. These results will be reported elsewhere in the near future.

The polyplex nanomicelles composed of PEG-b-P[Asp-(DET)] block copolymer and pDNA have demonstrated promising features for bone-regenerative gene therapy. The characteristics are summarized as: (i) good transfection efficiency with minimal cytotoxicity; (ii) sustained gene expression profile, which may be beneficial to cell differentiation; and (iii) excellent *in vivo* availability. Worth noting is that the enhancement of bone regeneration in this study was achieved without cell transplantation. Although the use of cell sources such as stem cells has been widely investigated, there remain many concerns for clinical application, such as the difficulty of finding an ideal cell source that meets both quality and quantity demands while also satisfying the concerns of medical costs and health risks.[44,45] Thus, it is desirable that cell transplantation be supplemented or replaced by innovations in other components of tissue engineering, signals, and scaffolds.

In conclusion, we developed a new gene delivery system applicable to bone regenerative medicine. This polyplex nanomicelle showed high biocompatibility as well as a capacity for regulated gene transfer, inducing a remarkable increase in the bone regeneration rate in a bone defect model. This system holds much promise for constructing a practical gene-activated matrix for tissue engineering. Moreover, this technology will help realize therapeutic applications of gene therapy requiring safe and regulated gene expressions.

MATERIALS AND METHODS

Materials. pDNAs encoding luciferase (pGL3-control, 5,256bp) (Promega, Madison, WI) and GFP (pEGFP-C1, 4,700bp) (Clontech, Palo Alto, CA) were amplified in competent DH5α *Escherichia coli* and purified using EndoFree Plasmid Maxi or Mega Kits (Qiagen, Hilden, Germany). pCMV5 pDNA expressing hemagglutinin-tagged mouse caALK6 and pcDEF3 pDNA expressing Flag-tagged mouse Runx2 were generous gifts from M. Krüppel (Mt. Sinai Hospital, Toronto, Canada) and K. Miyazono (University of Tokyo, Tokyo, Japan), respectively. The DNA concentration was determined by reading the absorbance at 260 nm. Commercially available transfection reagents, linear polyethylenimine (Exgen 500, M_w of LPEI = 22 kd) and FuGENE6 were purchased from MBI Fermentas (Burlington, Canada) and Roche (Basel, Switzerland), respectively. Dulbecco's modified Eagle's medium and fetal bovine serum were purchased from Sigma-Aldrich (St. Louis, MO).

Synthesis and characterization of PEG-b-P[Asp-(DET)] block copolymer. The PEG-b-P[Asp-(DET)] block copolymer was synthesized as previously reported.[24] Briefly, PEG-poly(β-benzyl-L-aspartate) (PEG-PBLA) diblock copolymer was synthesized by the ring-opening polymerization of β-benzyl-L-aspartate *N*-carboxy-anhydride from the terminal primary amino group of α-methoxy-ω-amino PEG (M_w: 12,000; Nippon Oil and Fats, Tokyo, Japan). The copolymer thus prepared was confirmed to be unimodal with a narrow molecular weight distribution (M_w/M_n: 1.23) by gel-permeation chromatography, and the number of repeating units of BLA was calculated to be 68 by ^{1}H-NMR (data not shown). The N-terminal amino group of PEG-PBLA was then acetylated using acetic anhydride in dichloromethane solution to obtain PEG-PBLA-Ac. The obtained polymer was dissolved in distilled *N,N*-dimethylformamide (Wako Pure Chemical Industries, Osaka, Japan) and reacted with diethylenetriamine (DET) (Tokyo Kasei Kogyo, Tokyo, Japan) for 24 hours at 40 °C under a dry argon atmosphere to undergo aminolysis of the benzyl side chain. After 24 hours, the solution was slowly dropped into 10% acetic acid solution and dialyzed (Spectra/por Membrane, molecular weight cut-off = 3,500, Rancho Dominquez, CA) against 0.01 N HCl and subsequently against distilled water. The final solution was lyophilized to obtain PEG-b-P[Asp-(DET)] as the hydrochloride salt form. ^{1}H-NMR confirmed the complete substitution of benzyl ester of the polymer with DET through the aminolysis reaction as well as the chemical structure of the obtained PEG-b-P[Asp-(DET)] block copolymer.

Preparation of pDNA carriers. The PEG-b-P[Asp-(DET)] block copolymer and pDNA were separately dissolved in 10 mmol/l Tris-HCl buffer (pH 7.4). Both solutions were mixed at various nitrogen/phosphate (= (total amines in cationic segment)/(DNA phosphates)) and left overnight. The pDNA complexes with LPEI and FuGENE6 were prepared by mixing the pDNA solution and the reagents following the protocols provided by the manufacturers.

In vitro *transfection.* HEK293 cells were obtained from the Riken Cell Bank (Tsukuba, Japan). Mouse calvarial cells were isolated from calvariae of neonatal littermates. The experimental procedures were in accordance with the guidelines of the Animal Committee of the University of Tokyo. Calvariae were digested for 10 minutes at 37 °C in an enzyme solution containing 0.1% collagenase and 0.2% dispase for five cycles. Cells isolated by the final four digestions were combined as an osteoblast population and cultured in Dulbecco's modified Eagle's medium containing 10% fetal bovine serum. Human synovial cells from rheumatoid arthritis patients were kindly provided by Dr. S. Tanaka (University of Tokyo).[46] Written informed consent for subsequent experiments was obtained from each patient.

For luciferase transfection assays, the cells were inoculated at a density of 2×10^4 cells/well in a 24-multiwell plate and cultured for 24 hours. After the culture medium was replaced with fresh medium containing 10% fetal bovine serum, pDNA carrier solution (33.3 μg/ml, 22.5 ml) was applied to each well. After several days of incubation, the cells were lysed and the luciferase gene expression was measured using a Luciferase Assay System (Promega, Madison, WI) and a Lumat LB9507 luminometer (Berthold, Bad Wildbad, Germany). The expression was normalized to protein concentrations of cell lysates. For the evaluation of sustained luciferase expression (Figure 4), the cells were seeded onto a 96-multiwell plate (6×10^3 cells/well). After incubation for 24 hours, 6 μl of each pDNA carrier solution was added, followed by further incubation for up to day 10. The luminescence was measured by a GloMax 96 Microplate Luminometer (Promega, Madison, WI). For the GFP transfection assay, both the phase contrast and the fluorescence images were obtained by an Axiovert 100 M microscope (Carl Zeiss, Oberkochen, Germany).

For the cytotoxicity assay, a 96-multiwell plate was used. After transfection as described above, the cells were incubated for 2 or 5 days and their viability was evaluated by an MTT assay (Cell Counting Kit-8, Dojindo, Kumamoto, Japan). Each well was measured by reading the absorbance at 450 nm according to the protocol provided by the manufacturer. The results were expressed as the relative value (%) of the control cells, which were incubated in parallel without transfection.

Evaluation of mRNA expression. After transfection to mouse calvarial cells, the total RNA was collected using the RNeasy Mini Preparation Kit (Qiagen, Hilden, Germany) according to the manufacturer's protocol. Gene expression was analyzed by quantitative PCR. Using the Quantitect SYBR Green PCR Kit (Qiagen, Hilden, Germany), 20 ng of total RNA was analyzed in a final volume of 20 μl according to the manufacturer's protocol. Reverse transcription was performed for 30 minutes at 50 °C followed by PCR: 40 thermal cycles of 15 seconds at 94 °C, 30 seconds at 55 °C, and 30 seconds at 72 °C using an ABI Prism 7500 Sequence Detector (Applied Biosystems, Foster City, CA). Each mRNA expression was normalized to levels of mouse β-actin mRNA, also determined by quantitative reverse transcription-PCR, from the same total RNA samples. The following primers were used: osteocalcin, forward primer (AAGCAGGAGGGC AATAAGGT) and reverse primer (TTTGTAGGCGGTCTTCAAGC); mouse ALK6, forward primer (CACCAAGAAGGAGGATGGAG) and reverse primer (CTAGACATCCAGAGGTGACAACAG); mouse Runx2, forward primer (CCCAGCCACCTTTACCTACA) and reverse primer (TATGGAGTGCTGCTGGTCTG); luciferase, forward primer (TTGA CCGCCTGAAGTCTCTGA) and reverse primer (ACACCTGCGTCGA AGATGTTG); mouse β-actin, forward primer (AGATGTGGATCAG CAAGCAG) and reverse primer (GCGCAAGTTAGGTTTTGTCA). As for luciferase, the gene expression presented as the light units was also evaluated in parallel.

In vitro *transfection from gene-containing scaffolds.* To prepare the scaffolds containing gene carriers, the PEG-P[Asp-(DET)]/pDNA micelles were mixed with calcium phosphate paste (BIOPEX-R; Mitsubishi Pharma, Osaka, Japan). According to the manufacturer's information, the powder consists of particles (2–5 mm in diameter) of α-tricalcium phosphate (75% wt), tetracalcium phosphate monoxide (18% wt), dicalcium phosphate dibasic (5% wt), and hydroxyapatite (2% wt); the aqueous solution contains sodium chondroitin sulfate (5.4%) and sodium succinate

(13%). For solidification, 1.0 g of the powder was manually mixed (at low shear rates) with 233 μl of the solution containing pDNAs. After solidification, the cement containing 1.3 μg of pDNA was placed onto the upper chamber of a BD Falcon Cell Culture Insert for 12-well plates (1.0 μm pore size, Becton Dickinson, Franklin Lakes, NJ), and HEK293 cells were plated onto the lower chamber. Five days later, luciferase assay was performed as described. The level of luciferase expression was normalized to the protein concentrations of cell lysates.

In vivo *gene delivery for the bone defect area on the mouse skull bone.* In this study, the 4 mm defects in diameter were chosen as the mouse bone defect model.[47,48] We have observed that the mouse calvarial defects (4 mm in diameter) could not be covered spontaneously with regenerated bone within 8 weeks after operation, although significant bone formation was observed at the defect edge (data not shown). Thus, the bone regeneration was evaluated within or at 4 weeks after gene delivery.

For the generation of bone defects, mice were anesthetized with ketamine/xylazine (80 mg/kg and 5 mg/kg) solution through intraperitoneal injection, and a linear incision was made along the sagittal suture from the frontal bone to the center of the occipital bone. A round craniotomy defect (4 mm in diameter) was manually created on both parietal bones with a sterile disposable trephine (Kai Industries, Gifu, Japan).[47] Calcium phosphate paste was used to fill in the defects, and then the incisions were sutured. The mice were killed at 2, 4, or 8 weeks after the operation for radiologic, histologic, or immunohistologic analyses, respectively. Animal experiments were performed according to the protocol approved by the Animal Care and Use Committee of the University of Tokyo.

Assessment of bone regeneration. After the mice were asphyxiated with carbon dioxide, the calvarias were removed. Tissue preparation, hematoxylin and eosin staining, and immunohistologic analysis using a rabbit polyclonal antibody against GFP (Molecular Probes, Eugene, OR) or a rabbit polyclonal antibody against type-I collagen (LSL, Tokyo, Japan) were performed as described.[49] To evaluate the extent of bone regeneration, serial coronal sections of the implantation site were performed at 0.5, 1, 1.5, 2, 2.5, 3, and 3.5 mm from the rostral end and then stained with hematoxylin and eosin. For each section, the original defect area and the regenerated bone area were measured by NIH Image software. The ratio of the summation of the regenerated bone area to that of the original defect area (SRBA/SODA) was calculated and used as the index of bone regeneration.

ACKNOWLEDGMENTS

We thank Michael Klüppel (Mount Sinai Hospital) and Kohei Miyazono (University of Tokyo) for pDNAs expressing caALK6 and Runx2, respectively. We also appreciate Sakae Tanaka (University of Tokyo) for providing human synovial cells. This work was supported by Grants-in-Aid for Scientific Research from the Japanese Ministry of Education, Culture, Sports, Science and Technology (#15390452 and #17390530), Health Science Research Grants from the Japanese Ministry of Health, Labor and Welfare (#H16-regenerative medicine-008), and the Core Research Program for Evolutional Science and Technology (CREST) from the Japan Science and Technology Corporation (JST).

SUPPLEMENTARY MATERIAL

Figure S1. Zeta-potential of polyplex nanomicelles and pDNA complexes with P[Asp-(DET)], the cationic segment of the block copolymer used in this study.

Figure S2. GFP gene expression in human synovial cells.

Figure S3. GFP gene expression in mouse calvarial cells.

Figure S4. *In vitro* transfection by polyplex nanomicelles incorporated into calcium phosphate cement scaffold.

REFERENCES

1. Bucholz, RW, Heckman, JD (2006). *Rockwood and Green's Fractures in Adults*. Lippincott Williams & Wilkins: Philadelphia, PA. 587pp.
2. Banwart, JC, Asher, MA and Hassanein, RS (1995). Iliac crest bone graft harvest donor site morbidity. A statistical evaluation. *Spine* **20**: 1055–1060.
3. Arrington, ED, Smith, WJ, Chambers, HG, Bucknell, AL and Davino, NA (1996). Complications of iliac crest bone graft harvesting. *Clin Orthop Relat Res* **329**: 300–309.
4. Langer, R and Vacanti, JP (1993). Tissue engineering. *Science* **260**: 920–926.
5. Bruder, SP and Caplan, AI (2000). *Principles of Tissue Engineering*. Academic Press: San Diego, CA. 683pp.
6. Winn, SR, Hu, Y, Sfeir, C and Hollinger, JO (2000). Gene therapy approaches for modulating bone regeneration. *Adv Drug Deliv Rev* **42**: 121–138.
7. Baltzer, AW and Lieberman, JR (2004). Regional gene therapy to enhance bone repair. *Gene Ther* **11**: 344–350.
8. Katagiri, T and Takahashi, N (2002). Regulatory mechanisms of osteoblast and osteoclast differentiation. *Oral Dis* **8**: 147–159.
9. Long, F, Chung, UI, Ohba, S, McMahon, J, Kronenberg, HM and McMahon, AP (2004). Ihh signaling is directly required for the osteoblast lineage in the endochondral skeleton. *Development* **131**: 1309–1318.
10. Komori, T (2003). Requisite roles of Runx2 and Cbfb in skeletal development. *J Bone Miner Metab* **21**: 193–197.
11. Patel, MS and Karsenty, G (2002). Regulation of bone formation and vision by LRP5. *N Engl J Med* **346**: 1572–1574.
12. Ogata, N, Chikazu, D, Kubota, N, Terauchi, Y, Tobe, K, Azuma, Y *et al.* (2000). Insulin receptor substrate-1 in osteoblast is indispensable for maintaining bone turnover. *J Clin Invest* **105**: 935–943.
13. Govender, S, Csimma, C, Genant, HK, Valentin-Opran, A, Amit, Y, Arbel, R *et al.* (2002). Recombinant human bone morphogenetic protein-2 for treatment of open tibial fractures: a prospective, controlled, randomized study of four hundred and fifty patients. *J Bone Joint Surg Am* **84-A**: 2123–2134.
14. Valentin-Opran, A, Wozney, J, Csimma, C, Lilly, L and Riedel, GE (2002). Clinical evaluation of recombinant human bone morphogenetic protein-2. *Clin Orthop Relat Res* **395**: 110–120.
15. Gerstenfeld, LC, Cullinane, DM, Barnes, GL, Graves, DT and Einhorn, TA (2003). Fracture healing as a post-natal developmental process: molecular, spatial, and temporal aspects of its regulation. *J Cell Biochem* **88**: 873–884.
16. Howell, TH, Fiorellini, J, Jones, A, Alder, M, Nummikoski, P, Lazaro, M *et al.* (1997). A feasibility study evaluating rhBMP-2/absorbable collagen sponge device for local alveolar ridge preservation or augmentation. *Int J Periodontics Restorative Dent* **17**: 124–139.
17. Zhao, M, Zhao, Z, Koh, JT, Jin, T and Franceschi, RT (2005). Combinatorial gene therapy for bone regeneration: cooperative interactions between adenovirus vectors expressing bone morphogenetic proteins 2, 4, and 7. *J Cell Biochem* **95**: 1–16.
18. Riew, KD, Wright, NM, Cheng, S, Avioli, LV and Lou, J (1998). Induction of bone formation using a recombinant adenoviral vector carrying the human BMP-2 gene in a rabbit spinal fusion model. *Calcif Tissue Int* **63**: 357–360.
19. Rutherford, RB, Moalli, M, Franceschi, RT, Wang, D, Gu, K and Krebsbach, PH (2002). Bone morphogenetic protein-transduced human fibroblasts convert to osteoblasts and form bone *in vivo*. *Tissue Eng* **8**: 441–452.
20. Schek, RM, Hollister, SJ and Krebsbach, PH (2004). Delivery and protection of adenoviruses using biocompatible hydrogels for localized gene therapy. *Mol Ther* **9**, 130–138.
21. Gafni, Y, Pelled, G, Zilberman, Y, Turgeman, G, Apparailly, F, Yotvat, H *et al.* (2004). Gene therapy platform for bone regeneration using an exogenously regulated, AAV-2-based gene expression system. *Mol Ther* **9**: 587–595.
22. Lundstrom, K (2003). Latest development in viral vectors for gene therapy. *Trends Biotechnol* **21**: 117–122.
23. Egermann, M, Lill, CA, Griesbeck, K, Evans, CH, Robbins, PD, Schneider, E *et al.* (2006). Effect of BMP-2 gene transfer on bone healing in sheep. *Gene Ther* **13**: 1290–1299.
24. Kanayama, N, Fukushima, S, Nishiyama, N, Itaka, K, Jang, WD, Miyata, K *et al.* (2006). A PEG-based biocompatible block catiomer with high buffering capacity for the construction of polyplex micelles showing efficient gene transfer toward primary cells. *ChemMedChem* **1**: 439–444.
25. Harada-Shiba, M, Yamauchi, K, Harada, A, Takamisawa, I, Shimokado, K and Kataoka, K (2002). Polyion complex micelles as vectors in gene therapy--pharmacokinetics and *in vivo* gene transfer. *Gene Ther* **9**: 407–414.
26. Itaka, K, Harada, A, Nakamura, K, Kawaguchi, H and Kataoka, K (2002). Evaluation by fluorescence resonance energy transfer of the stability of nonviral gene delivery vectors under physiological conditions. *Biomacromolecules* **3**: 841–845.
27. Itaka, K, Yamauchi, K, Harada, A, Nakamura, K, Kawaguchi, H and Kataoka, K (2003). Polyion complex micelles from plasmid DNA and poly(ethylene glycol)-poly(L-lysine) block copolymer as serum-tolerable polyplex system: physicochemical properties of micelles relevant to gene transfection efficiency. *Biomaterials* **24**: 4495–4506.
28. Boussif, O, Lezoualc'h, F, Zanta, MA, Mergny, MD, Scherman, D, Demeneix, B *et al.* (1995). A versatile vector for gene and oligonucleotide transfer into cells in culture and *in vivo*: polyethylenimine. *Proc Natl Acad Sci USA* **92**: 7297–7301.
29. Hellgren, I, Drvota, V, Pieper, R, Enoksson, S, Blomberg, P, Islam, KB *et al.* (2000). Highly efficient cell-mediated gene transfer using non-viral vectors and FuGene6: *in vitro* and *in vivo* studies. *Cell Mol Life Sci* **57**: 1326–1333.
30. Weiskirchen, R, Kneifel, J, Weiskirchen, S, van de Leur, E, Kunz, D and Gressner, AM (2000). Comparative evaluation of gene delivery devices in primary cultures of rat hepatic stellate cells and rat myofibroblasts. *BMC Cell Biol* **1**: 4.
31. Lee, MJ, Cho, SS, You, JR, Lee, Y, Kang, BD, Choi, JS *et al.* (2002). Intraperitoneal gene delivery mediated by a novel cationic liposome in a peritoneal disseminated ovarian cancer model. *Gene Ther* **9**: 859–866.
32. Elmadbouh, I, Rossignol, P, Meilhac, O, Vranckx, R, Pichon, C, Pouzet, B *et al.* (2004). Optimization of *in vitro* vascular cell transfection with non-viral vectors for *in vivo* applications. *J Gene Med* **6**: 1112–1124.
33. Tinsley, RB, Faijerson, J and Eriksson, PS (2006). Efficient non-viral transfection of adult neural stem/progenitor cells, without affecting viability, proliferation or differentiation. *J Gene Med* **8**: 72–81.
34. Ohba, S, Ikeda, T, Kugimiya, F, Yano, F, Lichtler, AC, Nakamura, K *et al.* (2007). Identification of a potent combination of osteogenic genes for bone

regeneration using embryonic stem (ES) cell-based sensor. *FASEB J* (epub ahead of print).
35. Hunter, AC (2006). Molecular hurdles in polyfectin design and mechanistic background to polycation induced cytotoxicity. *Adv Drug Deliv Rev* **58**: 1523–1531.
36. Bonadio, J, Smiley, E, Patil, P and Goldstein, S (1999). Localized, direct plasmid gene delivery *in vivo*: prolonged therapy results in reproducible tissue regeneration. *Nat Med* **5**: 753–759.
37. Verma, IM and Somia, N (1997). Gene therapy—promises, problems and prospects. *Nature* **389**: 239–242.
38. Bright, C, Park, YS, Sieber, AN, Kostuik, JP and Leong, KW (2006). *In vivo* evaluation of plasmid DNA encoding OP-1 protein for spine fusion. *Spine* **31**: 2163–2172.
39. Huang, YC, Simmons, C, Kaigler, D, Rice, KG and Mooney, DJ (2005). Bone regeneration in a rat cranial defect with delivery of PEI-condensed plasmid DNA encoding for bone morphogenetic protein-4 (BMP-4). *Gene Ther* **12**: 418–426.
40. Moghimi, SM, Symonds, P, Murray, JC, Hunter, AC, Debska, G and Szewczyk, A (2005). A two-stage poly(ethylenimine)-mediated cytotoxicity: implications for gene transfer/therapy. *Mol Ther* **11**: 990–995.
41. Geiger, F, Bertram, H, Berger, I, Lorenz, H, Wall, O, Eckhardt, C *et al.* (2005). Vascular endothelial growth factor gene-activated matrix (VEGF165-GAM) enhances osteogenesis and angiogenesis in large segmental bone defects. *J Bone Miner Res* **20**: 2028–2035.
42. Omidi, Y, Hollins, AJ, Benboubetra, M, Drayton, R, Benter, IF and Akhtar, S (2003). Toxicogenomics of non-viral vectors for gene therapy: a microarray study of lipofectin- and oligofectamine-induced gene expression changes in human epithelial cells. *J Drug Target* **11**: 311–323.
43. Kabanov, AV, Batrakova, EV, Sriadibhatla, S, Yang, Z, Kelly, DL and Alakov, VY (2005). Polymer genomics: shifting the gene and drug delivery paradigms. *J Control Release* **101**: 259–271.
44 Buttery, LD, Bourne, S, Xynos, JD, Wood, H, Hughes, FJ, Hughes, SP *et al.* (2001). Differentiation of osteoblasts and *in vitro* bone formation from murine embryonic stem cells. *Tissue Eng* **7**: 89–99.
45. Jiang, Y, Vaessen, B, Lenvik, T, Blackstad, M, Reyes, M and Verfaillie, CM (2002). Multipotent progenitor cells can be isolated from postnatal murine bone marrow, muscle, and brain. *Exp Hematol* **30**: 896–904.
46. Seto, H, Kamekura, S, Miura, T, Yamamoto, A, Chikuda, H, Ogata, T *et al.* (2004). Distinct roles of Smad pathways and p38 pathways in cartilage-specific gene expression in synovial fibroblasts. *J Clin Invest* **113**: 718–726.
47. Hirata, K, Tsukazaki, T, Kadowaki, A, Furukawa, K, Shibata, Y, Moriishi, T *et al.* (2003). Transplantation of skin fibroblasts expressing BMP-2 promotes bone repair more effectively than those expressing Runx2. *Bone* **32**: 502–512.
48. Cowan, CM, Shi, YY, Aalami, OO, Chou, YF, Mari, C, Thomas, R *et al.* (2004). Adipose-derived adult stromal cells heal critical-size mouse calvarial defects. *Nat Biotechnol* **22**: 560–567.
49. Kugimiya, F, Kawaguchi, H, Kamekura, S, Chikuda, H, Ohba, S, Yano, F *et al.* (2005). Involvement of endogenous bone morphogenetic protein (BMP) 2 and BMP6 in bone formation. *J Biol Chem* **280**: 35704–35712.

In Vivo Antitumor Activity of the Folate-Conjugated pH-Sensitive Polymeric Micelle Selectively Releasing Adriamycin in the Intracellular Acidic Compartments

Younsoo Bae,[†,‡] Nobuhiro Nishiyama,[†,‡] and Kazunori Kataoka*[,†,‡,§]

Center for Disease Biology and Integrative Medicine, Graduate School of Medicine, The University of Tokyo, 7-3-1 Hongo, Bunkyo-ku, Tokyo 113-0033, Japan, and Center for NanoBio Integration and Department of Materials Engineering, The University of Tokyo, 7-3-1 Hongo, Bunkyo-ku, Tokyo 113-8656, Japan. Received December 26, 2006; Revised Manuscript Received March 2, 2007

Cancer treatment efficacy and safety of the environmentally sensitive polymeric micelle drug carriers were significantly increased by optimizing the number of ligands on their surface. These micelles were designed to target the cancerous tumors through the interaction between folate and its receptors that overexpress on the cancer cell membrane while achieving pH-controlled drug release in the intracellular acidic compartments such as endosomes and lysosomes. In order to elucidate the effects of folate on cytotoxicity, biodistribution, anticancer activity, and pharmacological properties, folate concentration on the surface of the micelles was controlled by precise synthesis of two different amphiphilic block copolymers that self-assemble into spherical micelles, folate–poly(ethylene glycol)–poly(aspartate-hydrazone-adriamycin) with γ-carboxylic acid activated folate and methoxy-poly(ethylene glycol)–poly(aspartate-hydrazone-adriamycin) without folate. It is of significance that, although folate conjugation induced an extremely small change in tumor accumulation of the micelles, folate-conjugated micelles showed lower in vivo toxicity and higher antitumor activity over a broad range of the dosage from 7.50 to 26.21 mg/kg, which was 5-fold broader than free drugs.

INTRODUCTION

Precise control of the amount and uniform distribution of ligands on nanoparticles is one of the most challenging assignments in the design of polymeric drug carriers for successful active drug targeting (*1*–*3*). Indeed, a large number of studies have shown that active drug targeting is promising for effective cancer treatment (*4*–*7*). However, the questions about how many ligands are necessary for achieving efficient active drug targeting of the polymeric drug carriers are still controversial and remain to be elucidated further. In particular, when such drug carriers are tailored to deliver anticancer drugs to cancer cells systemically, it is of significant importance to confirm whether the ligand conjugation maintains their pharmacokinetic properties without decreasing antitumor activity. It is because anticancer drugs are normally highly toxic, inducing serious side effects, and although ligands can increase the interaction between the drug carriers and targeted cells in the body, they might also induce an increase in the cellular interaction with nontargeted cells, that we are not willing to deliver drugs. In order to answer these questions, we have to prepare first a drug carrier with optimal amounts of ligands, whose chemical and biological properties are fairly well established and then ascertain whether ligand installation induces any change in its biological properties.

The rationales for tumor-specific drug delivery with polymers have been reported during the past decades and are based on the characteristics of tumor tissues such as disordered and leaky vasculatures, a thick extracellular matrix, and other microenvironmental peculiarities including the hypoxic environment, expression of cancer-specific receptors, and excessive secretion of cytokines (*8*–*9*). One of the widely accepted methodologies for polymeric drug delivery is to target leaky tumor vessels and the poorly developed lymphatic drainage in the tumor tissues so that polymers and their drug conjugates can pass the tumor blood vessel wall and then accumulate in tumor tissue for a prolonged time. This methodology is explained as the enhanced permeability and retention (EPR) effect, providing the most probable theory for passive drug targeting (*10*). Nevertheless, recent studies have revealed that tumor-targeting drug delivery cannot be completely achieved only by the EPR effect because polymeric drug carriers often encounter difficulties in accessing cancer cells in the deeper place of the tumor tissues or in interacting with the targeted cells after accumulation (*11*, *12*). Polymeric drug carriers are normally required to have biocompatibility and high molecular weight to prevent protein adsorption that induces recognition by the body defense system and to increase the tumor accumulation via the EPR effect, respectively. However, these efforts frequently result in low cellular uptake of polymeric drug carriers after extravasation, reducing the actual drug concentration within the tumor due to the stagnation around the tumor tissue. As a result, we should inject polymeric drug carriers with a higher amount compared to free drugs to deliver a sufficient amount of drugs to the tumor. This is also the reason the current polymeric drug delivery systems urgently need to improve their targeting efficiency. From these aspects, active targeting has been believed to clear the problems by facilitating polymeric drug delivery systems (*13*). Active targeting can be achieved by installing ligands to the polymers or polymer assemblies so that they can interact with receptors that express on the targeted sites such as cancer cell membranes. Nevertheless, it is obvious that active targeting

* To whom correspondence should be addressed: Kazunori Kataoka, Ph.D. Professor, Department of Materials Engineering, Graduate School of Engineering, The University of Tokyo, 7-3-1 Hongo, Bunkyo-ku, Tokyo 113-8656, Japan. Phone +81-3-5841-7138, Fax +81-3-5841-7139, E-mail: kataoka@bmw.t.u-tokyo.ac.jp.

† Graduate School of Medicine.

‡ Center for NanoBio Integration.

§ Department of Materials Engineering.

10.1021/bc060401p CCC: $37.00
Published on Web 05/09/2007

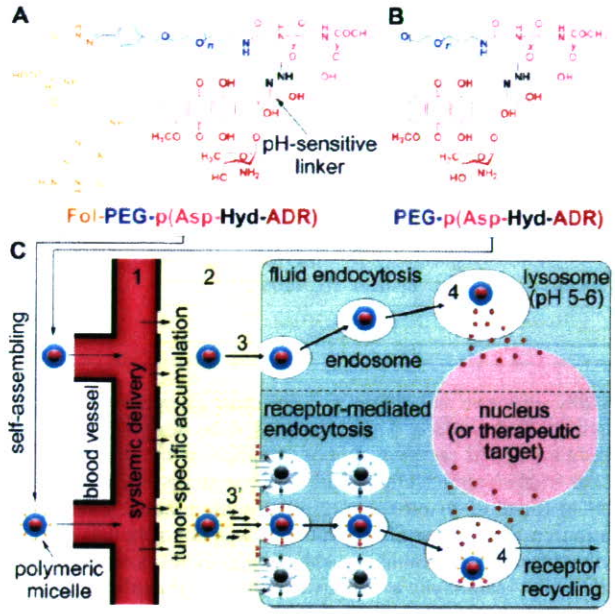

Figure 1. Design of polymeric micelles and the rationale for active drug delivery. Chemical structures of folate−poly(ethylene glycol)−poly(aspartate-hydrazone-adriamycin) and methoxy-poly(ethylene glycol)−poly(aspartate-hydrazone-adriamycin) block copolymers (A and B). As shown in panel C, these polymers can self-assemble into the polymeric micelles that can effectively achieve systemic drug delivery and tumor-specific accumulation (1 and 2). The micelles are then uptaken by the cancer cells via fluid endocytosis (3) or receptor-mediated endocytosis (3′) depending on surface design for accelerating endocytosis (e.g., folate conjugation). Anticancer drugs, adriamycin (ADR), that are conjugated through a pH-sensitive hydrazone bond can be released from the micelles in the acidic intracellular compartments such as endosomes or lysosomes where pH ranges from 5 to 6 (4).

cannot be achieved until passive targeting of drug carriers is successfully accomplished.

Amphiphilic block copolymers are useful tools for the preparation of supramolecular assemblies. By precisely controlling their molecular weight and the hydrophilic/hydrophobic balance, we can prepare spherical supramolecular nanoassemblies, also known as "the polymeric micelles", with a hydrophilic shell that envelopes a hydrophobic core (*14*). The polymeric micelle is considered to be one of the most successful polymeric drug carrier formulations, because it is characterized by high drug loading contents, prolonged blood circulation, and selective tumor accumulation (*15*). Most notably, their chemical, biological, and pharmacological properties have been widely studied, and thus we can easily investigate the effect of active targeting (*16, 17*). In this study, poly(ethylene glycol)−poly(β-benzyl-L-aspartate) block copolymers (PEG−PBLA) were synthesized for the basic platform for the preparation of the polymeric micelles, and these micelles were further functionalized to conjugate anticancer drugs and ligands. Figure 1 shows the chemical structures of the block copolymers used in this study. Anticancer drugs, adriamycin (ADR), were conjugated to the side chains of the core-forming poly(aspartic acid) block through a hydrazone linkage, which can be selectively cleaved under the acidic conditions with pH ranging from 5 to 6, corresponding to the intracellular vesicles such as the endosomes and lysosomes (*18*). In our previous studies, we have reported that this intracellular pH-sensitive polymeric micelle showed remarkably low toxicity and high in vivo efficacy (*19*). It was also confirmed that the pH-sensitive micelles can release drugs selectively by responding to a decrease in intracellular pH of the cell, and therefore, drug leakage from the micelles decreases during the blood circulation and tumor-specific drug delivery efficiency increases. In the meantime, folate was conjugated at the end of the shell-forming poly(ethylene glycol) (PEG) block for active targeting. Folate, an anionic form of folic acid, is a vitamin B9 that helps the production and maintenance of new cells. Originally, folate was necessary for the restoration of the DNA damage that may induce cancer. However, interestingly, cancer cells overexpress folate-binding proteins (FBPs) on their cell membranes (*20, 21*). This is probably due to the DNA replication that is supported by folate, which is also a prerequisite for the cancer growth. More interestingly, cancer cells are believed to reduce chemotherapeutical response by regulating intracellular folate concentration (*22*). Therefore, we can actively guide polymeric drug carriers to cancer cells in the body by folate conjugation (*23*). It must be noticed that FBP binding activity of folate drastically changes depending on its activated state, which is distinguished by an inactive α- and active γ-carboxyl activated form (*24*). Herein, we conjugated folate to PEG at its γ-carboxyl position to maintain its activity by precision synthesis as reported elsewhere (*25*−*27*).

The objectives of this research are to ascertain whether folate conjugation can enhance antitumor efficacy of the pH-sensitive micelles without deteriorating the characteristics of the micelles as a long-circulating drug carrier with high tumor accumulation, and to determine how much folate concentration is optimum for achieving effective passive and active drug targeting simultaneously. Such information would be beneficial to the future design and preparation of ligand-installed multifunctional polymeric drug carriers for cancer treatment.

EXPERIMENTAL PROCEDURES

Materials and Devices. Acetic anhydride (AA), chloroform ($CHCl_3$), *N,N*-dimethyl formamide (DMF), dimethyl sulfoxide (DMSO), hexane, methanol (MeOH), methanesulfonyl chloride (CH_3SO_2Cl), triethylamine (TEA), trifluoroacetic acid (TFA), trifluoroacetic anhydride (TFAA), and tetrahydrofuran (THF) were purchased from Wako Pure Chemical Industries, Japan. DMF, hexane, and THF were distilled twice following standard procedures. Carbazic acid *tert*-butyl ester (CAt-BE) and potassium carbonate (K_2CO_3) were purchased from Tokyo Kasei Organic Chemicals, Japan. These chemicals were used without further purification. Daunorubicin (DAU), folic acid (Fol), 4-(diethoxymethyl)benzaldehyde, and sodium borohydride ($NaBH_4$) were purchased from Sigma Chemical, U.S.A. Ethylene oxide (EO) was from Sumitomo Seika Chemicals, Japan, and dried over calcium hydride followed by distillation. β-Benzyl-L-aspartate (BLA) was from Sigma, and α-methoxy-ω-amino-poly(ethylene glycol) (MeO-PEG-NH_2) was from Nippon Oil and Fats, Japan. PEG was purified using an ion-exchange gel column (CM-Sephadex C-50, Amersham Pharmacia Biotech, U.S.A.) prior to the synthesis of the block copolymers. Adriamycin hydrochloride (ADR) was kindly provided by Nippon Kayaku, Japan, and its purity was checked by reversed-phase liquid chromatograpy (RPLC). Sephadex LH-20 gel was from Amersham Pharmacia Biotech, Sweden. Gel permeation chromatography (GPC) analysis was carried out using a TOSOH HLC-8220 equipped with TSK-GEL columns (G4000PWXL and G3000PWXL). Internal refractive index (RI) and ultraviolet−visible absorption (UV) detectors were used. DMF containing 10 mM of LiCl was used as an eluant at a flow rate of 0.8 mL/min at 40 °C. ^1H NMR spectra were measured with a JEOL EX300 spectrometer (JEOL, Japan). Flow cytometric analysis was performed with EPICS XL Flow Cytometry Systems (Beckman Coulter, U.S.A.). The multimode reader Mithras LB 940 (Berthold Technologies, U.S.A.) was used for in vitro cytotoxicity evaluation using a CellTiter-Glo luminescent cell viability assay kit (Promega, U.S.A.).

Cell Lines and Animals. A human pharyngeal cancer cell line KB was purchased from Health Science Research Resources Bank, Japan. Cells were cultured in Dulbecco's Modified Eagle cell culture Medium (DMEM, Sigma, U.S.A.) containing 10% FBS under a humidified atmosphere with 5% CO_2 at 37 °C. CD-1 nude mice (female, 6-week-old) were purchased from Charles River, Japan. The animals were cared for and all experiments were performed in compliance with the Guide for the Care and Use of Laboratory Animals as adopted and promulgated by the National Institutes of Health. The number of independent experiments is stated as n, and the experimental data are expressed as mean and mean ± SEM for relative and absolute values, respectively.

Synthesis of Self-Assembling Amphiphilic Block Copolymers. In this study, we synthesized two different types of self-assembling amphiphilic block copolymers for the preparation of the micelles, folate−poly(ethylene glycol)−poly(aspartate-hydrazone-adriamycin) [Fol−PEG−p(Asp-Hyd-ADR)] and methoxy-poly(ethylene glycol)−poly(aspartate-hydrazone-adriamycin) [PEG−p(Asp-Hyd-ADR)]. Synthesis methods for these block copolymers were previously reported elsewhere (*25*). Briefly, Fol−PEG−p(Asp-Hyd-ADR) was synthesized via seven steps as follows.

a. Synthesis of Heterobifunctional α-4-(Diethoxymethyl)-benzylacetal-ω-amine-poly(ethylene glycol) (aceBz-PEG-NH_2). 4-(Diethoxymethyl)benzaldehyde (5 g) was reduced with $NaBH_4$ (1 g) in dry ethanol (100 mL). Obtained 4-(diethoxymethyl)-benzylalcohol (0.19 g) was then mixed with potassium naphthalene (115 mg) in dry THF (30 mL) to prepare potassium 4-(diethoxymethyl)benzylalkoxide, followed by the addition of distilled EO (11.9 g) for anionic polymerization to obtain aceBz-PEG-OH. After 2 days of reaction at 25 °C, CH_3SO_2Cl (0.62 g) and TEA (0.82 g) were added to aceBz-PEG-OH in 25 mL of THF to prepare an intermediate product aceBz-PEG-OSO_2CH_3, which was then mixed with ammonia solution (25%) to produce aceBz-PEG-NH_2.

b. Selective Functionalization of Folic Acid at its γ-Position of the Glutamate Residue with Hydrazide (Fol-hyd). An excess amount of TFAA (3 mL) was added dropwisely to folic acid (2 g) in THF (20 mL) to prepare N_{10}-(trifluoroacetyl)pyrofolic acid. This pyrofolic acid (500 mg) was reacted with CAt-BE (1.6 g) in 20 mL of dry DMF at 40 °C overnight. Prepared folate-hydrazide-BOC was treated with TFA to obtain Fol−Hyd.

c. Preparation of β-benzyl-L-aspartate N-Carboxy Anhydride (BLA−NCA). 5.77 g of triphosgene was added to 10 g of β-benzyl-L-aspartate in 150 mL of dry THF at 40 °C, and the reaction was allowed to proceed until the solution became clear. Prepared β-benzyl-L-aspartate *N*-carboxy anhydride (BLA−NCA) was purified by recrystallization from hexane.

d. Ring-Opening Polymerization of BLA−NCA by Using aceBz-PEG-NH_2 as a Macroinitiator to Obtain 4-(Diethoxymethyl)benzyl Acetal−poly(ethylene glycol)−poly(β-benzyl-L-aspartate) (aceBz−PEG−PBLA). 6 g of aceBz−PEG−NH_2 with molecular weight of 12 000 and 5 g of BLA−NCA were dissolved in 30 mL and 10 mL of DMSO, respectively. NCA solution was added to PEG solution at 40 °C, and the reaction was allowed to proceed for 2 days.

e. ω-Amino Group Protection for aceBz−PEG−PBLA Block Copolymers, Followed by α-Acetal Group Deprotection and Subsequent Conjugation of Fol−hyd at the End of the PEG Chain (Fol−PEG−PBLA). The ω-amino group of aceBz−PEG−PBLA was protected by AA to prevent dimerization between aldehyde−benzyl−poly(ethylene glycol)−poly(β-benzyl-L-aspartate) (CHO−Bz−PEG−PBLA) block copolymers, which can be prepared by deprotecting acetal groups of aceBz−PEG−PBLA with 0.1 N HCl aqueous solution. End-group protected CHO−Bz−PEG−PBLA (250 mg) was then mixed with Fol−Hyd (50 mg) in dry DMF to prepare Fol−PEG−PBLA.

f. Substitution Benzyl Esters at the Side Chain of Fol−PEG−PBLA with Drug-Binding Hydrazide Groups to Prepare Fol−PEG−p(Asp-Hyd). 500 mg of Fol−PEG−PBLA was dissolved in 10 mL of dry DMF, and anhydrous hydrazine (0.62 mg) was added to the solution. The reaction was allowed to proceed at 40 °C for 2 h, followed by deprotection of remained benzyl groups with 0.1 N NaOH aqueous solution at 25 °C. Polymers were dialyzed against 0.25% ammonia solution and collected by freeze-drying.

g. Conjugation of ADR at Its 13-C Carbonyl with the Hydrazide Groups of Fol−PEG−p(Asp-Hyd) through a pH-Sensitive Schiff Base Linkage. Fol−PEG−p(Asp-Hyd) (100 mg) in 50 mL of DMSO was mixed with an excess amount of ADR-HCl (100 mg) with respect to drug-binding hydrazide residues. The mixed solution was stirred at room temperature for 3 days. After precipitation from ether, Fol−PEG−p(Asp-Hyd-ADR) was redissolved in 10 mL of DMF and purified by gel filtration using a Sephadex LH-20 column. In the case of PEG−p(Asp-Hyd-ADR), MeO-PEG-NH_2 was used as a macroinitiator for BLA−NCA polymerization at step (d) instead of aceBz−PEG-NH_2, following the procedures from steps (e) to (g).

Table 1. Polymer Compositions

compound	composition[a]	polydispersity index[d] (Mw/Mn)	drug loading content (wt %)
PEG-PBLA	12−42[b]	1.12	
Fol-PEG-PBLA	12−40[b]	1.14	
PEG-p(Asp-Hyd-ADR)	12−42−33−15[c]		33.84
Fol-PEG-p(Asp-Hyd-ADR)	12−40−34−14[c]		34.32

[a] The compositions of the block copolymers are abbreviated *X*−*Y* and *X*−*Y*−*Z*−*A*. The letter *X* stands for molecular weight × 10^{-3} of poly(ethylene glycol), while *Y*, *Z*, and *A* denote the numbers of aspartic acid, hydrazide, and adriamycin (ADR), respectively. [b] The values were calculated from the peak area ratio determined by ^{1}H NMR between poly(ethylene glycol) and benzyl groups of the PBLA block. [c] The numbers of hydrazide groups and ADR were determined by ^{1}H NMR and reversed-phase liquid chromatography (RPLC), respectively. [d] Polydispersity was measured for PEG−PBLA and Fol−PEG−PBLA to ensure the purity of starting materials.

Preparation of the Folate-Conjugated pH-Sensitive Polymeric Micelles. The folate-conjugated pH-sensitive polymeric micelles were prepared from Fol−PEG−p(Asp-Hyd-ADR) alone or in combination with PEG−p(Asp-Hyd-ADR) block copolymers in various molar ratios to change folate contents (0%, 1%, 2%, 5%, 10%, 25%, 50%, and 100%). We distinguish the micelles from Fol−PEG-p(Asp-Hyd-ADR) and PEG−p(Asp-Hyd-ADR) by the notations of FMA and MA, which denote folate-conjugated micellar adriamycin and micellar adriamycin, respectively. For the preparation of FMA and MA, 250 mg of each Fol−PEG−p(Asp-Hyd-ADR) and PEG−p(Asp-Hyd-ADR) were dissolved in 5 mL of DMSO. Polymer solutions were then added dropwise into 95 mL of Tris−HCl buffer solution (10 mM, pH 7.4), sonicated at 25 °C for 10 min, and diluted further with 900 mL of Tris−HCl buffer. The polymer solutions were concentrated by Amicon Ultra-15 Centrifugal Filter Units (Millipore, U.S.A.) with molecular weight cutoff (MWCO) 30 000 kDa. 12 mL of the solutions in each swinging bucket rotor were spun at 1500 *g* at 25 °C for 15 min. During repetitive centrifugation, additional Tris−HCl buffer was added to the solutions until DMSO was completely removed. Concentrated micelle solutions were filter-sterilized and stored in aliquots at 4 °C for future use. Drug concentration was determined by UV at 490 nm, based on the calibration curve of free ADR.